2-P

OPTICAL POLARIMETRIC PROPERTIES OF THE ECHO II AND PAGEOS I ENGINEERING SURFACES

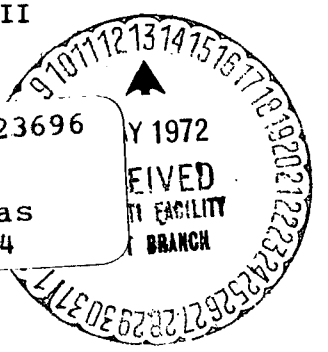

A Thesis

Presented To

the Faculty of the School of Engineering and Applied Science

University of Virginia

In Partial Fulfillment

of the Requirements for the Degree

Master of Engineering Physics

---

by

Robert Benjamin Lee, III

June 1972

ACKNOWLEDGMENTS

The author is indebted to the National Aeronautics and Space Administration for permission to use material obtained from a research project at the Langley Research Center in this thesis. Particular thanks are due Mr. Gerald M. Keating for his guidance during this investigation.

The author is also grateful to Drs. Ralph A. Lowry and John K. Haviland for their comments and suggestions in preparing this thesis. The author wishes to thank his wife, Margaret, for her patience, encouragement, and support during the last five years.

APPROVAL SHEET

This thesis is submitted in partial fulfillment of

the requirements for the degree of

Master of Engineering Physics

Robert Benjamin Lee, III
Author

Approved:

Ralph A. Lowry
Faculty Adviser

Dean, School of Engineering and
Applied Science

June 1972

TABLE OF CONTENTS

LIST OF FIGURES

FIGURES PAGE

FIGURES PAGE

SYMBOLS

A	defined by equation (31)
$\bar{A}$	difference in azimuths of sun and satellite, degree
Az	azimuth
Alt	altitude
a	angle between observer's zenith and polar axis of telescope, degree
B	blue spectral band, having an effective wavelength of 0.44 μm
B	defined by equation (32)
b	angle between observer's zenith and polar axis of telescope, degree
C	cross-sectional area, square centimeter
D	distance from test sphere to detector, meter
E	maximum amplitude of electric vector
E_M	amplitude of polarized electric vector
F	force, Newton
$F(\psi)$	Russell phase function, defined by equation (21)
f	focal length, centimeter
h	height of surface roughness, micrometer
I_i	intensity of incident light, lumen/centimeter^2
I_M	polarized component of light intensity, lumen/centimeter^2
I_o	unpolarized component of light intensity, lumen/centimeter^2
I_{max}	maximum intensity of light measured behind a polarization analyzer, lumen/centimeter^2

I_{min}	minimum intensity of light measured behind a polarization analyzer, lumen/centimeter^2
I_p	intensity of light vibrating parallel to plans of incidence, lumen/centimeter^2
I_s	intensity of light vibrating perpendicular to plane of incidence, lumen/centimeter^2
I_x	intensity of light vibrating parallel to active axis of Wollaston prism, lumen/centimeter^2
$I_{x'}$	intensity of light vibrating parallel to active axis of half-wave plate, lumen/centimeter^2
I_y	intensity of light vibrating perpendicular to axis of Wollaston prism, lumen/centimeter^2
$I_{y'}$	intensity of light vibrating perpendicular to active axis of half-wave plate, lumen/centimeter^2
I_1	intensity component of light transmitted through Wollaston prism, lumen/centimeter^2
I_2	intensity component of light transmitted through Wollaston prism, lumen/centimeter^2
k_o	coefficient of absorption
l_j	dimension of plane surface facet, centimeter
N	complex index of refraction
N_j	local surface normal to plane surface facet
N_o	mean surface normal
N'	direction of polar axis for telescope

n	real index of refraction
O	culmination point of satellite
P	percent polarization
r	radius of curvature, centimeter
S	stress, newton/centimeter^2
U	ultraviolet spectral band, effective wavelength of 0.36 μm
V	visual spectral band, effective wavelength of 0.55 μm
v	photovoltage, millivolt
x	distance measured along mean surface to some point on a rough surface, micrometer
Y	defined by equation (A.34)
Y_i	observed values of polarization
Z	zenith
z_1, z_2, z_3	coefficients in quadratic equation (30)
α	angle between plane of polarization and optical axis of polarization analyzer, degree
β	relative angle of analyzer with respect to declination axis of telescope, degree
γ	diffusely reflected fraction of incident light
ϵ_j	angle measured clockwise from N_o to N_j, degree
η	angle of polarization, measured counter-clockwise from plane of incidence to plane of polarization in degrees
η_1	angle between plane of polarization and declination axis of telescope, degree

Θ	Principal Angle of Incidence, degree
θ_p	Brewster's angle, degree
θ_1	angle of incidence, measured counter-clockwise from N_o to incident light beam in degree
θ_1'	angle of reflection, measured clockwise from N_o to reflected light beam, in degrees
θ_2	angle of refraction, measured counter-clockwise from N_o to refracted beam of light in degrees
Λ	wavelength of a rough surface measured between periodic features in micrometer
λ	wavelength of light, micrometer
π	constant 3.14
ρ	specularly reflected fraction of incident light
ϕ	phase difference between two components E_x' and E_y'
ψ	phase angle, measured between the incident and reflected light beams in degrees
ω	angular frequency

Subscripts:

B	denotes blue spectral band
M	polarized
o	unpolarized
P	denotes direction parallel to plane of incidence
S	denotes direction perpendicular to plane of incidence
U	denotes ultraviolet spectral band

V	denotes visual spectral band
x	refers to direction along active axis of Wollaston prism
x'	refers to direction along active axis of half-wave plate
y	refers to direction perpendicular to active axis of Wollaston prism
y'	refers to direction perpendicular to active axis of half-wave plate

Superscript:

	refers to reflected light

ABSTRACT

Experimental investigations of the percent polarization of sunlight reflected from the surfaces of each the Echo II Satellite and PAGEOS (Passive Geodetic Earth Orbiting Satellite) were performed to determine the stability of their surfaces in the space environment. The Echo II surface material was amorphous phosphate chemically bonded to a rolled aluminum substrate while the PAGEOS I surface material is vapor deposited aluminum on a poly (ethylene terephthalate) film. The stability of the satellites' surfaces was analyzed by comparing the light polarizing properties of the satellites, measured by means of the NASA Satellite Photometric Observatory,to those of test surfaces representative of the satellites' surfaces. The properties of flat test surfaces were measured experimentally in the laboratory, and the effects of surface strain, surface geometry, and vacuum upon these properties were examined. The laboratory analyses revealed that the polarization properties of the Echo II surface were significantly affected by surface geometry and vacuum, and that the properties of the PAGEOS I surface were not significantly altered by any of the above mechanisms. The comparison of the laboratory data to those of the satellites indicated that the Echo II Satellite experienced detectable changes in its optical polarization properties during its five year lifetime in space, and that the PAGEOS I surface experienced little, if any, surface degradation during its first three years in the space environment, indicating it to be stable.

CHAPTER I

INTRODUCTION

The Echo II satellite (figure 1) was a 41.15-meter-diameter inflatable balloon having a reflecting surface of an amorphous phosphate coating formed on a rolled aluminum foil substrate. It was launched in 1964 as part of a passive satellite communication program (Ref. 1) and was used in the National Geodetic Satellites Program (NGSP) described in Reference 2. The PAGEOS I (Passive Geodetic Earth Orbiting Satellite), figure 2, is a 30.48-meter-diameter inflatable balloon having a highly reflective surface of aluminum vapor-deposited on a poly (ethylene terephthalate) film. It was launched in June 1966 as part of the NGSP.

The Echo II and PAGEOS I were initially polarimetrically measured during the winter of 1967 to explore the use of the percent polarization of sunlight reflected from them to evaluate the stability of their optical surfaces, exposed to the long-term effects of the space environment. These measurements were performed using the NASA Satellite Photometric Observatory (Ref. 3) in the ultraviolet U, blue B, and visual V spectral bands as a function of phase angle (angle formed between the directions of the incident and reflected light).

The percent polarization of light reflected from a surface is dictated by its optical constants and surface finish as well as the phase angle. Thus, it was felt that changes occurring in the surfaces of the satellites could be deduced from careful polarization measurements of the sunlight reflected from them.

Figure 1.- Fully inflated 41.15-meters-diameter Echo II.

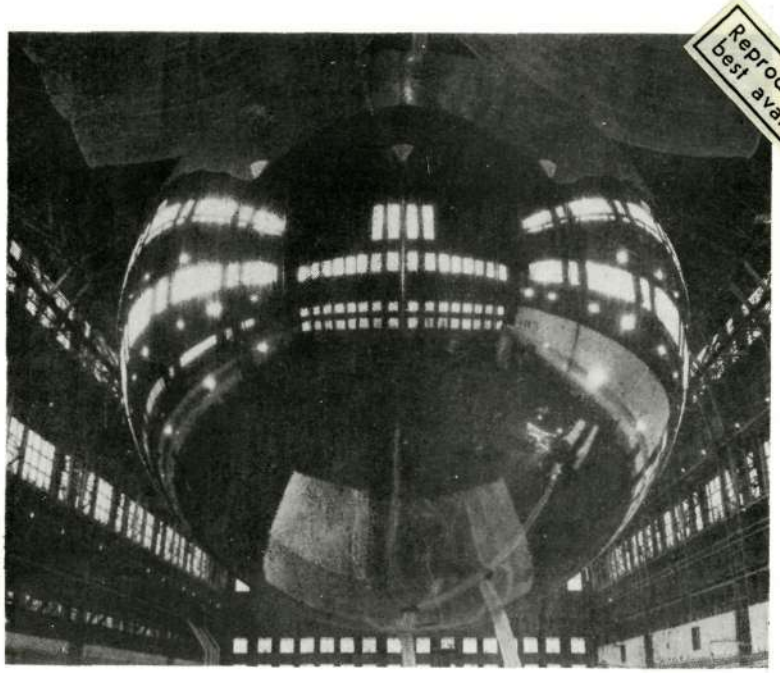

Figure 2.- Fully inflated 30.48-meters-diameter PAGEOS I.

Since it was not possible to have observed the satellites when they were initially launched, the approach in the evaluation of their surfaces has been to use the basic light polarizing properties of flat test surfaces representative of these satellites as references. The initial comparisons of the basic polarization properties of the test materials, determined in the laboratory, to those measured for the satellites in 1967 emphasized the need to obtain satellite measurements at phase angles greater than 130°. These necessary data were obtained during the winter of 1969. The later comparisons of the laboratory data to the 1969 satellite data indicated that they significantly differed. Thus, more detailed laboratory investigations were conducted to determine whether the satellites had experienced surface degradation and whether certain mechanisms were responsible for the observed differences.

In this paper, the effects of skin strain, surface geometry, and vacuum upon the light polarizing properties of the flat test surfaces are explored experimentally. The laboratory data are compared to the satellite data in order to deduce changes occurring in the surface properties of the satellites.

It should be mentioned that the satellite polarization measurements were obtained under Contracts NAS1-6436 and -8276 and reported in References 4 and 5, and that the determination of the optical constants for the satellite surfaces was not attempted since the Observatory is not capable of making this type of determination.

CHAPTER II

THEORY

The percent polarization of light reflected from flat surfaces which are optically smooth and rough are discussed. The polarization expected from spheres is explored based on the specular and diffuse reflecting characteristics of the basic reflecting surface.

Flat Surfaces

Optically smooth surfaces. - Dielectrics and metals introduce linear and elliptical polarization components to light reflected from them. The dominant vibration direction and plane of polarization, containing the polarized component of the light, for the specularly reflected light are generally found perpendicular to the plane of incidence (plane defined by the direction of the incident light beam and surface normal). The percent polarization P of the specularly reflected light is defined by the following equation.

$$P = \frac{\rho_s - \rho_p}{\rho_s + \rho_p} \times 100\% \qquad (1)$$

where ρ_s and ρ_p represent the reflected fractions of the incident light vibrating perpendicular and parallel to the plane of incidence.

For optically smooth dielectrics, ρ_s and ρ_p can be described by Fresnel's formulas (Ref. 6) as

$$\rho_s = \left[\frac{-\mathrm{Sin}(\theta_1 - \theta_2)}{\mathrm{Sin}(\theta_1 + \theta_2)}\right]^2 \tag{2}$$

and

$$\rho_p = \left[\frac{\mathrm{Tan}(\theta_1 - \theta_2)}{\mathrm{Tan}(\theta_1 + \theta_2)}\right]^2 \tag{3}$$

where θ_1 and θ_2 are the angles of incidence and refraction, respectively (see figure 3). The average reflected fraction ρ is assumed to be equal to the average of ρ_s and ρ_p. That is

$$\rho = \frac{\rho_s + \rho_p}{2} \tag{4A}$$

or

$$\rho = \frac{1}{2}\left[\frac{-\mathrm{Sin}(\theta_1 - \theta_2)}{\mathrm{Sin}(\theta_1 + \theta_2)}\right]^2 + \frac{1}{2}\left[\frac{\mathrm{Tan}(\theta_1 - \theta_2)}{\mathrm{Tan}(\theta_1 + \theta_2)}\right]^2 \tag{4B}$$

Looking at equation (4B), it can be seen that the ρ_p term goes to zero when $\theta_1 + \theta_2 = 90°$, leaving the reflected light completely plane polarized perpendicular to the plane of incidence. The angle of incidence where this occurs is called Brewster's angle θ_p, and is defined in terms of the real index of refraction n as

$$\theta_p = \tan^{-1} n \tag{5}$$

For angles of incidence other than Brewster's angle θ_p, the reflected light is partially plane-polarized. The equations (2) and (3) can be simplified by applying Snell's law

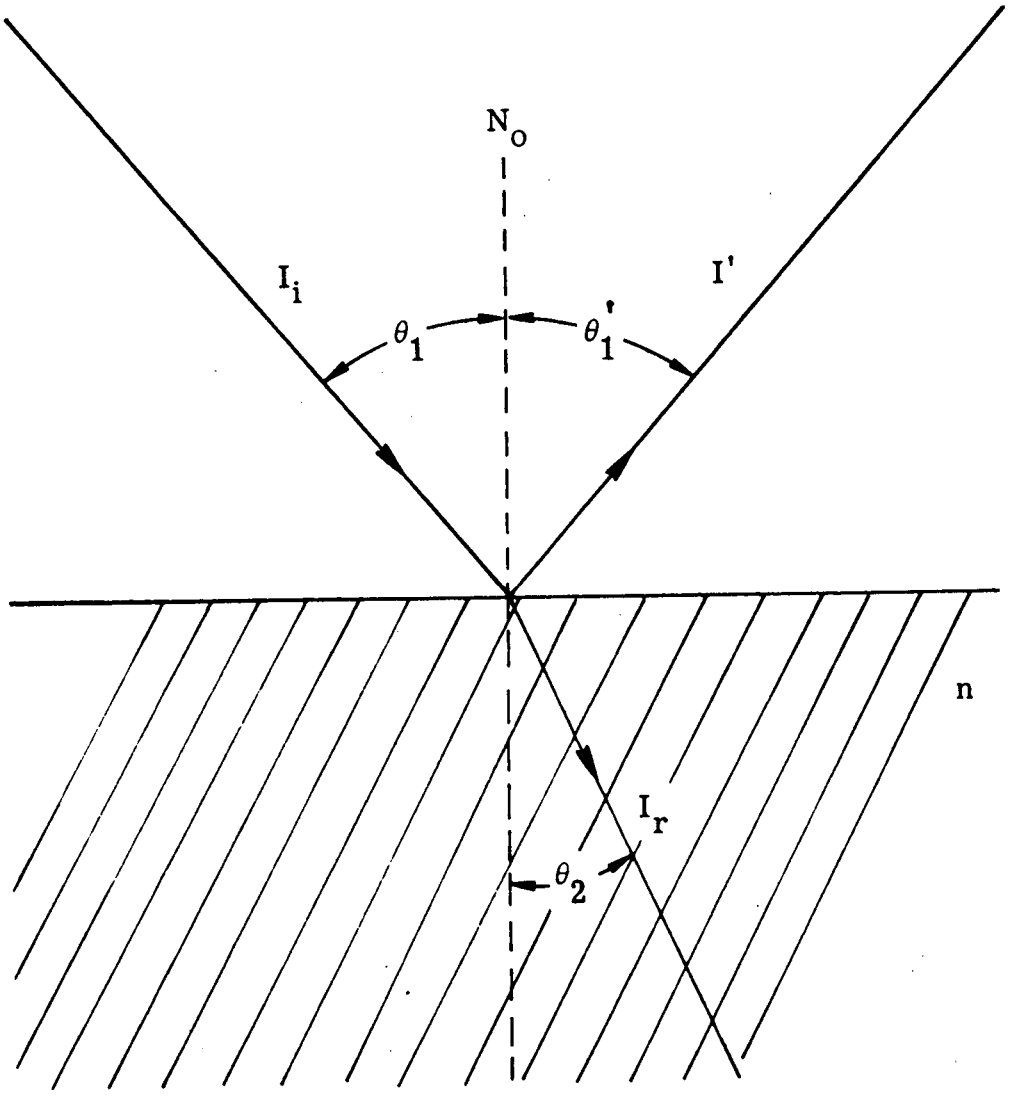

Figure 3.- Dieletric reflecting surface.

$$n = \frac{\sin \theta_1}{\sin \theta_2} \tag{6}$$

to

$$\rho_s = \left[\frac{\mathrm{Cos}(\theta_1) - n\mathrm{Cos}(\theta_2)}{\mathrm{Cos}(\theta_1) + n\mathrm{Cos}(\theta_2)}\right]^2 \tag{7}$$

$$\rho_p = \left[\frac{n\mathrm{Cos}(\theta_1) - \mathrm{Cos}(\theta_2)}{n\mathrm{Cos}(\theta_1) + \mathrm{Cos}(\theta_2)}\right]^2 \tag{8}$$

For optically smooth metals, ρ_s and ρ_p can be calculated by substituting the complex index of refraction N

$$N = n - ik_o \tag{9}$$

for n in equations (7) and (8), where k_o is the coefficient of absorption (see Ref. 6). The resulting equations are

$$\rho_s = \frac{\left[(n - \mathrm{Cos}(\theta_1)\right]^2 + k_o^2}{\left[(n + \mathrm{Cos}(\theta_1)\right]^2 + k_o^2} \tag{10}$$

and

$$\rho_p = \frac{\left[\left(n - \frac{1}{\mathrm{Cos}(\theta_1)}\right]^2 + k_o^2\right.}{\left[n + \frac{1}{\mathrm{Cos}(\theta_1)}\right]^2 + k_o^2} \tag{11}$$

which are valid when $n^2 + k_o^2$ is large compared to unity. In analogy to Brewster's angle, the angle of incidence for metals where ρ_p is a minimum, but not zero, is called the Principal Angle of Incidence Θ. The reflected light at Θ is elliptically polarized.

When the reflecting surface consists of a semitransparent dielectric coated to a metal, it would be expected that the reflected light would be a combination of linear polarization from the dielectric and elliptical polarization from the metal. The polarization of the reflected light should be more sensitive to the optical constants of the dielectric than those of the metal if the dielectric is coated to a significant thickness and its optical constants are not of the order of those for the metal. Also, there are interference effects to consider where the coating thickness is of the order of the wavelength λ of the incident light.

Rough surfaces. - Surfaces which are rough reflect light incident upon them in all directions as well as in the specular direction. Such rough surfaces are classified as either periodic or random. The periodically roughened surface exhibits periodic variations in the amplitude of the surface roughness, measured from the plane of the mean surface, while the randomly roughened surfaces are exhibits random variations in the amplitude (Ref. 7). The periodically roughened surface is of interest in this paper because the Echo II and its aluminum substrate materials exhibit this type of surface roughness. In the following paragraphs, the effect of periodic surface roughness will be briefly explored.

Consider the rough surface, figure 4, to consist of a semi-infinite surface which variation in amplitude $h(x)$ can be described by

$$h(x) = h \ \mathrm{Cos} \ \left(\frac{2\pi x}{\Lambda}\right) \tag{12}$$

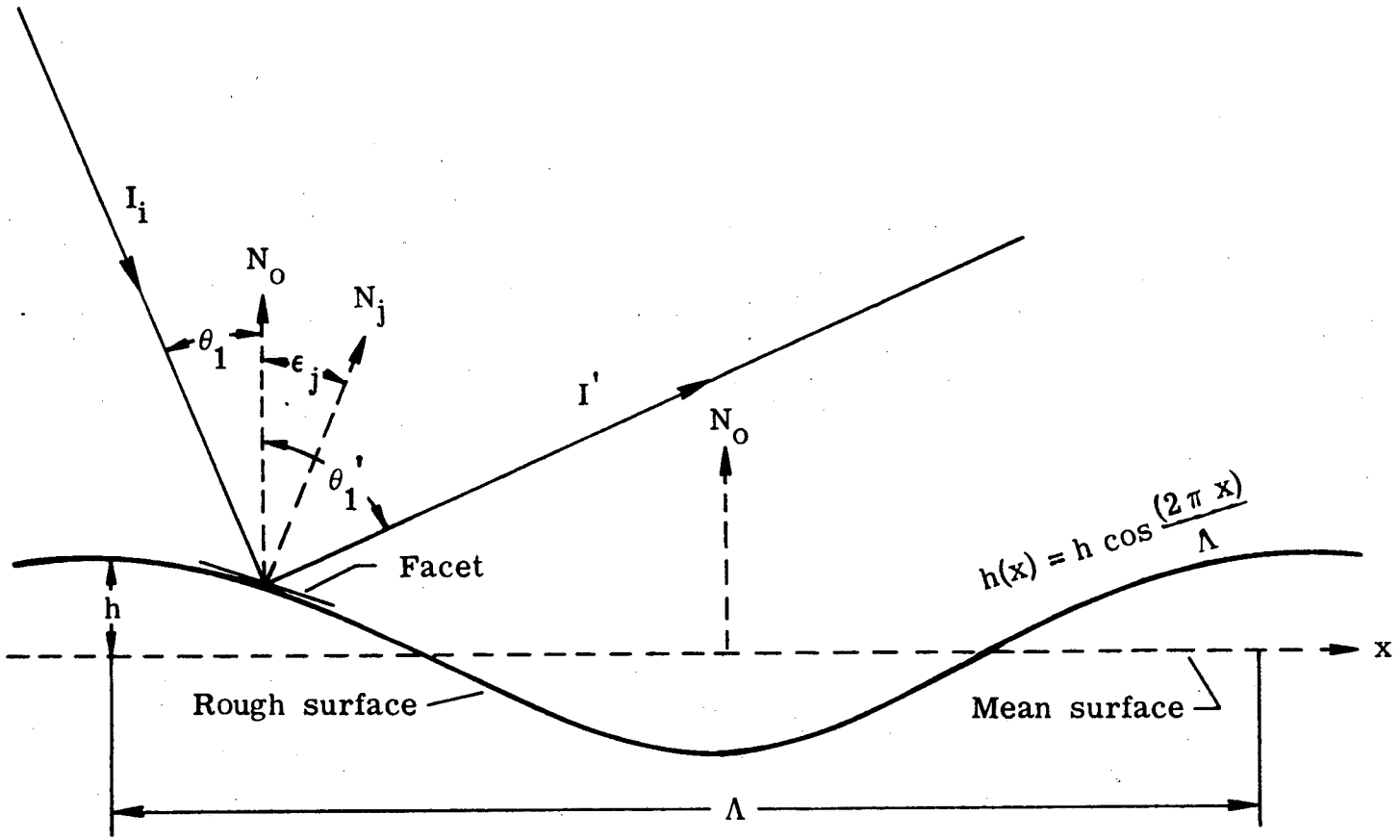

Figure 4.- Schematic diagram of a periodically rough surface.

where h is the amplitude of surface roughness, Λ is the wavelength of the periodic surface features, and x is the distance measured along the mean surface. The surface is assumed to be formed by numerous plane facets whose dimensions ℓ_j are large compared to the wavelength λ of the incident light (Ref. 8). The angle between the macronormal N_o for the mean surface and the local surface normal N_j to each facet is ε_j, measured clockwise from N_o; the surface normals N_j's are assumed to be coplanar and lie in the plane of incidence.

The incident light is projected upon the rough surface at an angle of incidence θ_1, measured counterclockwise from N_o. The light reflected from the surface at an angle of reflection θ_1', measured clockwise from N_o, is collected by a detector located at far-field. The reflected light should consist of specularly reflected light from a limited number of parallel facets, multiple (double reflection) reflected light, and diffusely reflected light. The intensities of the reflected light vibrating perpendicular I_s' and parallel I_p' to the plane of incidence can be expressed as

$$I_s' = \Sigma\rho_s(\theta_1)I_i 1_j \cos\theta_1 + \Sigma\rho_s^2(\theta_1 + \varepsilon_j)\cos^2(\theta + \varepsilon_j)I_i 1_j \qquad (13)$$

$$+ \gamma_s I_i \bar{I} \cos\theta_1 \Delta\theta_1'$$

$$I_p' = \Sigma\rho_p(\theta_1)I_i 1_j \cos\theta_1 + \Sigma\rho_p^2(\theta_1 + \varepsilon_j)\cos^2(\theta_1 + \varepsilon_j)I_i 1_j \qquad (14)$$

$$+ \gamma_p I_i \bar{I} \cos\theta_1 \Delta\theta_1'$$

where I_i is the intensity of the incident light, γ is the coefficient for diffuse reflection, and $\Delta\theta_1'$ is the solid angle subtended by the diffusely reflected light which is collected at the detector. The first term in each of equations (13) and (14) refer to specularly reflected light; the second term to multiple reflected light which includes double reflection in the specular direction; and the third term refers to diffusely reflected light. The polarization can be defined by substituting equations (13) and (14) into the following equation

$$P = \frac{I_s' - I_p'}{I_s' + I_p'} \times 100 \qquad (15)$$

Looking at equations (13) and (14), if multiple and diffuse reflection do not occur, the polarization of the specularly reflected light would be

$$P = \frac{\Sigma\rho_s(\theta_1)\mathrm{Cos}(\theta_1)I_i 1_j - \Sigma\rho_p(\theta_1)\mathrm{Cos}(\theta_1)I_i 1_j}{\Sigma\rho_s(\theta_1)\mathrm{Cos}(\theta_1)I_i 1_j + \Sigma\rho_p(\theta_1)\mathrm{Cos}(\theta_1)I_i 1_j} \qquad (16A)$$

or

$$P = \frac{[\rho_s(\theta_1) - \rho_p(\theta_1)]}{[\rho_s(\theta_1) + \rho_p(\theta_1)]} \times 100$$

Comparing equation (16B) to (1), it can be seen they are the same, indicating the use of the Fresnel formulas when $h << \lambda << \Lambda$. When diffusely reflected light occurs as well as specularly reflected light, the polarization is

$$P = \frac{\Sigma\,[\rho_s(\theta_1) - \rho_p(\theta_1)]}{\Sigma[\rho_s(\theta_1) + \rho_p(\theta_1)] + (\gamma_s + \gamma_p)\Delta\theta_1'} \times 100 \qquad (17)$$

Comparing (17) to (1), it can be seen that the polarization is reduced assuming the diffusely reflected light to be unpolarized $(\gamma_s = \gamma_p)$. When multiple reflection is considered, the polarization is found to be greater than that for specular reflection. This is because the ρ_s component is enhanced more than the ρ_p component resulting in

$$\frac{\rho_p^2(\theta_1 + \varepsilon_1)}{\rho_s^2(\theta_1 + \varepsilon_1)} < \frac{\rho_p(\theta_1)}{\rho_s(\theta_1)} \qquad (18)$$

In addition, the polarization will obtain its maximum value at an angle of incidence less than that expected for specular reflected light from a smooth surface. Generally it is expected that the nonspecularly or diffusely reflected light will be polarized due to multiple reflection of the light for $\theta_1' \neq \theta_1$.

Spherical Surfaces

The polarization of light reflected from a sphere is dependent upon the specular and diffuse reflectances of the basic reflecting surface. The equations (References 9, 10 and 11) predicting the intensities I_s' and I_p' are given below

$$I_s' = \frac{1}{4}\rho_s(\theta_1)I_i(r/D)^2 + \frac{2}{3}\gamma_s I_i(r/D)^2 F(\psi) \qquad (19)$$

$$I_p' = \frac{1}{4}\rho_p(\theta_1)I_i(r/D)^2 + \frac{2}{3}\gamma_p I_i(r/D)^2 F(\psi) \tag{20}$$

where

$$F(\psi) = \left[\frac{\mathrm{Sin}(\psi) + (\pi - \psi)\mathrm{Cos}(\psi)}{\pi}\right] \tag{21}$$

ψ is the angle formed between the incident and the reflected light beams ($\psi = 2\theta_1$), r is the radius of curvature for the sphere, and D is the distance from the sphere to the detector (D >> r). The polarization of the light reflected from a sphere can be calculated by substituting eqs. (19) and (20) into eq. (15). The resulting polarization equation is

$$P = \frac{(\rho_s - \rho_p) + \frac{8}{3}F(\psi)(\gamma_s - \gamma_p)}{(\rho_s + \rho_p) + \frac{8}{3}F(\psi)(\gamma_s + \gamma_p)} \times 100 \tag{22}$$

For the case of a sphere reflecting the light specularly where γ_s and γ_p are zero, the polarization equation becomes

$$P = \frac{\frac{1}{4}I_i(r/D)^2(\rho_s - \rho_p)}{\frac{1}{4}I_i(r/D)^2(\rho_s + \rho_p)} \times 100 \tag{23A}$$

which reduces to

$$P = \frac{\rho_s - \rho_p}{\rho_s + \rho_p} \times 100 \tag{23B}$$

Comparing eq. (23B) to eq. (16B) for a flat specularly reflecting surface, it can be seen that they are the same, emphasizing that the

polarization is independent of geometric shape for a specularly reflecting surface. Also, the polarization of light reflected from a diffusely reflecting sphere should be the same as that reflected from a diffusely reflecting, flat surface where ρ_s and ρ_p are zero. When a sphere reflects a significant component of diffuse light as well as specular light, the polarization can be described by the following equation

$$P = \frac{\rho_s - \rho_p}{\rho_s + \rho_p + \frac{8}{3}(\gamma_s + \gamma_p)F(\psi)} \times 100 \qquad (24)$$

assuming $\gamma_s = \gamma_p$.

Comparing equation (24) to equation (17) for a flat surface reflecting both specularly and diffusely, it can be seen that the sphere should polarize the incident light less than the flat surface would. This indicates that the polarization would be dependent upon the geometric shape of the reflecting surface in this particular case.

Angle of polarization. - In working with polarized light, the angle of polarization η, defining the orientation of the plane of incidence to the plane of polarization (containing the polarized component of the reflected light), is another parameter useful in describing the polarized light. The angle of polarization as it was pointed out earlier in this chapter is generally found to be 90 degrees for light reflected from flat dielectric and metallic surfaces. For the cases of specularly and diffusely reflecting spheres, the angle of polarization should be 90 degrees if ρ_s is greater than ρ_p and if γ_s is greater than γ_p. For the case of a sphere reflecting both specularly and

diffusely, the angle of polarization should be 90° if $\rho_s > \rho_p$ and if $\gamma_s > \gamma_p$. However, if γ_p is greater than γ_s, then the angle of polarization can be described by the following equation

$$\eta = \text{Tan}^{-1} \frac{\frac{1}{8}(\rho_s - \rho_p)}{\frac{1}{3}(\gamma_p - \gamma_s)F(\psi)} \tag{25}$$

Looking at eq. (25), it can be seen that the angle of polarization will be less than 45° if the polarization component for the diffusely reflected light is greater than that for the specularly reflected light. This would result in the polarization of the reflected light being negative, looking at eq. (22). If the polarization component of the diffuse light is less than that for the specular light, then the angle of polarization will be greater than 45°, and the polarization of the light will be positive. The above mentioned trends have been observed for sunlight reflected from the lunar surface (Ref. 12).

CHAPTER III

TEST MATERIALS

Description of Materials

The materials investigated are representative of the Echo II (Ref. 13) and PAGEOS I (Ref. 14) surfaces.

The Echo II material is an alodine (amorphous phosphate) coating chemically bonded to the outer surfaces of an aluminum-PET (polyethylene terephthalate) - aluminum substrate. The alodine, a semitransparent dielectric, was coated with an average density of 1.99×10^{-4} gm/cm^2. The substrate is composed of a 8.89-μm-thick PET film adhesively bonded between two layers of 4.57-μm-thick rolled aluminum foil. The foil has a surface line structure (figure 5) which is prominent even when it is coated (Reference 15). The reflecting surface for the Echo II material is the alodine coated to the aluminum foil.

The PAGEOS I material is a 0.22-μm-thick aluminum layer vapor-deposited on one side of a 12.70-μm-thick PET film. The reflecting surface is the aluminum.

Surface Geometry

The test materials had flat and spherical reflecting surfaces. The flat surfaces were obtained by placing the materials in a sample holder, resembling an embroidery hoop, under stress. The spherical surfaces were obtained by mounting the materials in 1.27 cm wide gores

on 12.70-cm-diameter spheres, figure 6(a). The spheres had 1.51 centimeter diameter polar caps. The surface line structures for the Echo II and its substrate materials were oriented along the length of the gores figure 6(b).

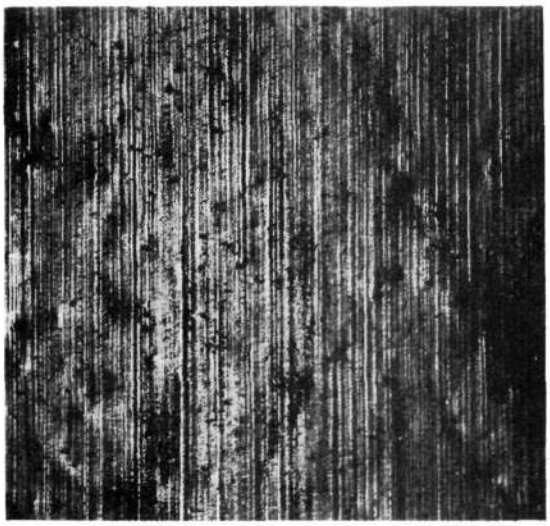

Figure 5.- Micrograph of the Echo II aluminum-foil substrate, illustrating the surface line structure. Micrograph made in oblique light at 50 x magnification.

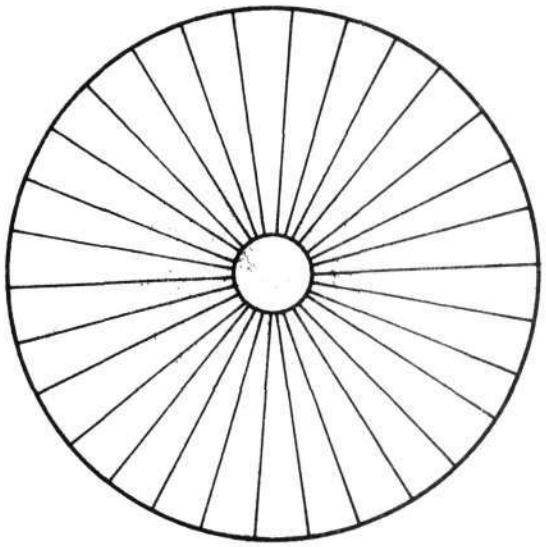

a.- Gores and polar cap.

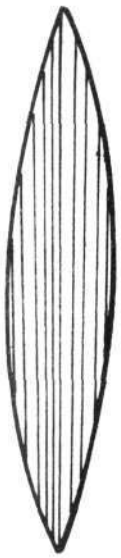

b.- Orientation of surface line structure along gore.

Figure 6.- Test sphere.

CHAPTER IV

LABORATORY TESTS

Tests were performed to investigate the effects of strain, surface geometry, and vacuum upon the light polarizing properties of the test materials. In the following paragraphs, the polarization measurements and tests are described.

Polarization Measurements

The polarization of light reflected from the test materials was measured as a function of phase angle ψ and spectral band using a planar goniophotometer equipped with linear analyzers. The goniophotometer is discussed in Reference 16 and will be briefly described here. The goniophotometer consisted of source, detection, and sample units as shown in figure 7. The source unit was located on the stationary arm of the apparatus while the detection unit was mounted on the movable arm having an axis of rotation which allowed the phase angle ψ to be varied from 10° to 180°, and which confined the measurements to the plane of incidence. The sample unit was mounted to a turntable which had an axis of rotation common to that of the movable arm. This axis allowed the angle of incidence θ_1 to be varied from -90° to +90°. Components of the apparatus are described in table I. The effective wavelengths of the light measured in the ultraviolet, blue, and visual spectral bands were 0.36, 0.44, and 0.55 micrometer.

The light path in the apparatus is illustrated in figure 8. A collimated light beam is projected upon the test material at a

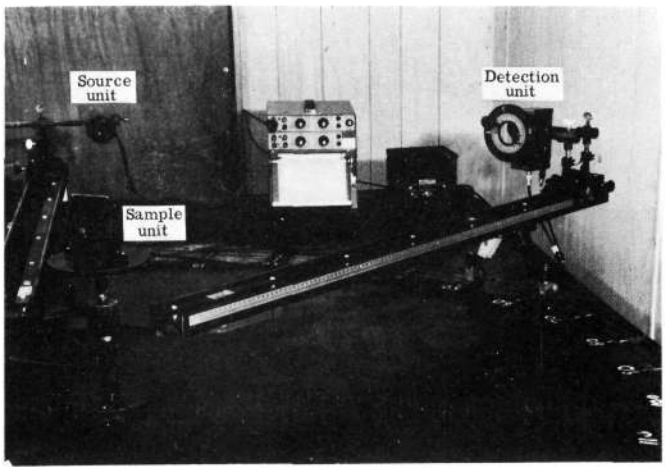

Figure 7.- Photograph of goniophotometer.

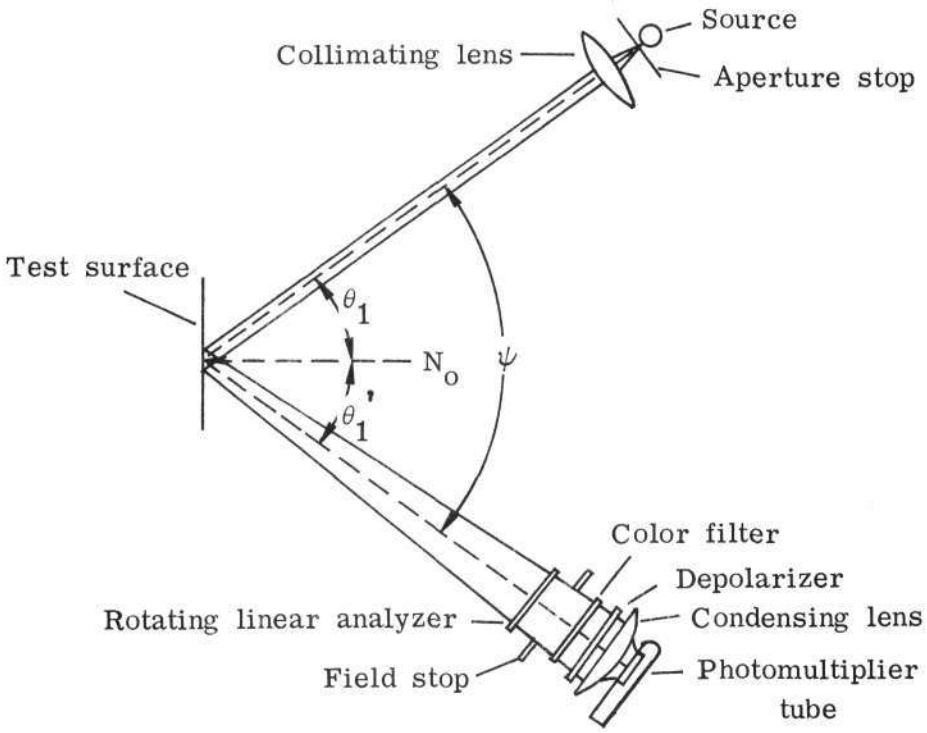

Figure 8.- Light path in the goniophotometer.

TABLE I. - COMPONENTS OF GONIOPHOTOMETER

Component	Description
Source	Zirconium concentrated arc lamp
Aperture Stop	0.1-cm-diameter opening
Collimating lens	Fused quartz, focal length = 10.00 cm
Rotating linear analyzer	HNB'P (ultraviolet) and HN38 (blue and visual)
Field Stop	2.0-cm-diameter opening
Color Filter	Standard astronomical ultraviolet, blue, and visual
Depolarizer	Lyot, constructed of two calcite discs, 0.15 and 0.20-cm-thick, cemented with their optical axes at 45°
Condensing lens	Fused quartz, focal length = 8.30
Photomultiplier tube	RCA 1P21, S-4 response

preselected angle of incidence θ_1. Then, the light, specularly reflected ($\theta_1 = \theta_1'$) from the test material at a preselected phase angle ψ, is passed through a rotating linear analyzer, field stop, color filter, depolarizer, and then is focused onto the entrance slit of the photomultiplier tube. When the light was polarized, the resulting photovoltage varied as the $\cos^2\alpha$ where α is the angle through which the analyzer was rotated beyond the plane of polarization (plane where the maximum light transmission occurs through the analyzer), figure 9(a). The variation of the photovoltage v with α can be described by the following equation

$$v = v_M \cos^2\alpha + v_o \tag{26}$$

where v_M and v_o are the amplitudes of the photocurrent corresponding to the polarized I_M and unpolarized I_o fluxes of the reflected light. The angle α and the variation of v with α are depicted in figure 9(a). Looking at the figure , it can be seen that v reached its maximum value, v_{max}, when α was equal to 0° or 180°, and that v obtained its minimum value, v_{min}, when α was equal to 90° or 270°. Since v_{max} and v_{min} corresponded to the maximum I_{max} and the minimum I_{min} intensities of the reflected light, the percent polarization P of the light was determined by substituting v_{max} and v_{min} into the following equation

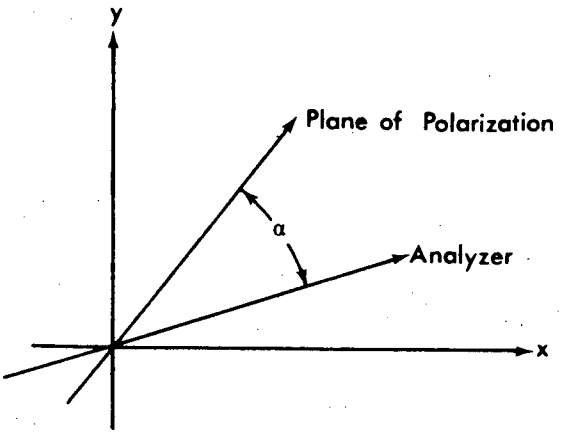

a. Angle α

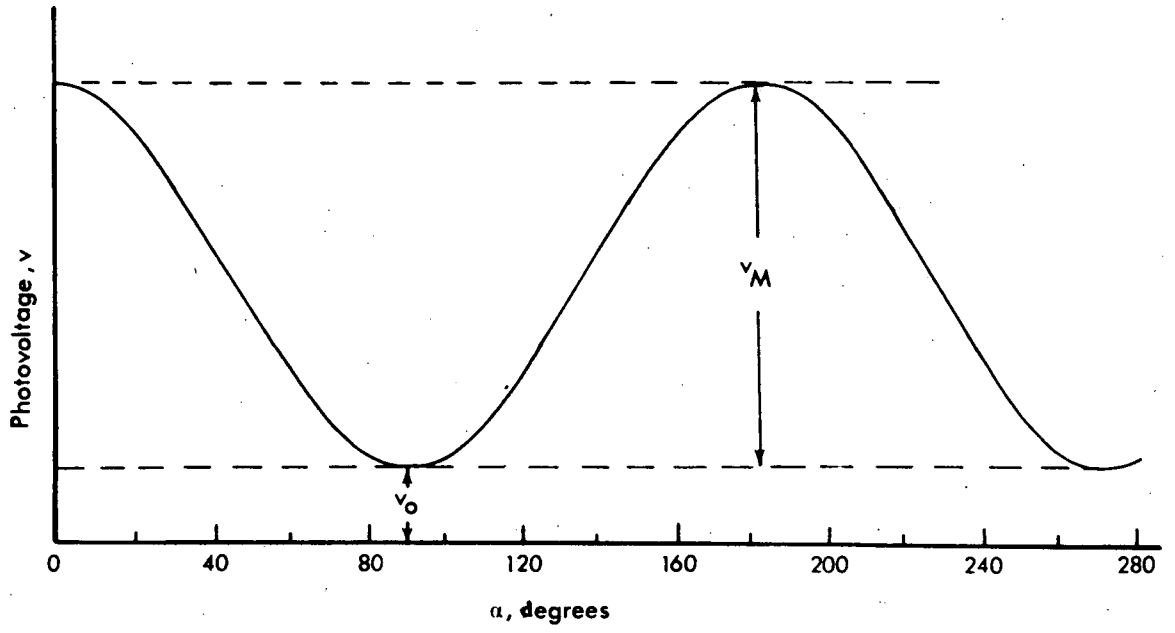

b. Variation of the photovoltage v with angle α

Figure 9.- Angle α and variation of the photovoltage with the angle α.

$$P = \frac{v_{max} - v_{min}}{v_{max} + v_{min}} \times 100 \qquad (27)$$

Using this method, the percent polarization and the angle of polarization were determined from the photovoltage v and the angle α.

The reliability of the apparatus to produce reasonable polarization measurements was determined by measuring the percent polarization of zinc crown glass and comparing the results to those predicted for the glass. The experimental data are compared to the theoretical data in figure 10. The theoretical data were calculated using equations (1), (7), and (8) and assuming $n = 1.52$ (Ref. 17). The comparison indicates that the apparatus produces reasonable values for the polarization.

Stress - Relaxation Test

The test materials were subjected to uniaxial stress by applying loads to 7.62 by 45.72 cm strips of the test materials for two week periods, and then allowing the strips to relax for a week with no load applied to simulate inflation conditions that the PAGEOS and Echo II experienced during their first two weeks in orbit. The stress applied was determined using the following equation

$$S = \frac{F}{C} \qquad (28)$$

where F is the force of the load, and C is the cross-sectional area (thickness times width) of the strip. Forces of 6.575 and 0.448

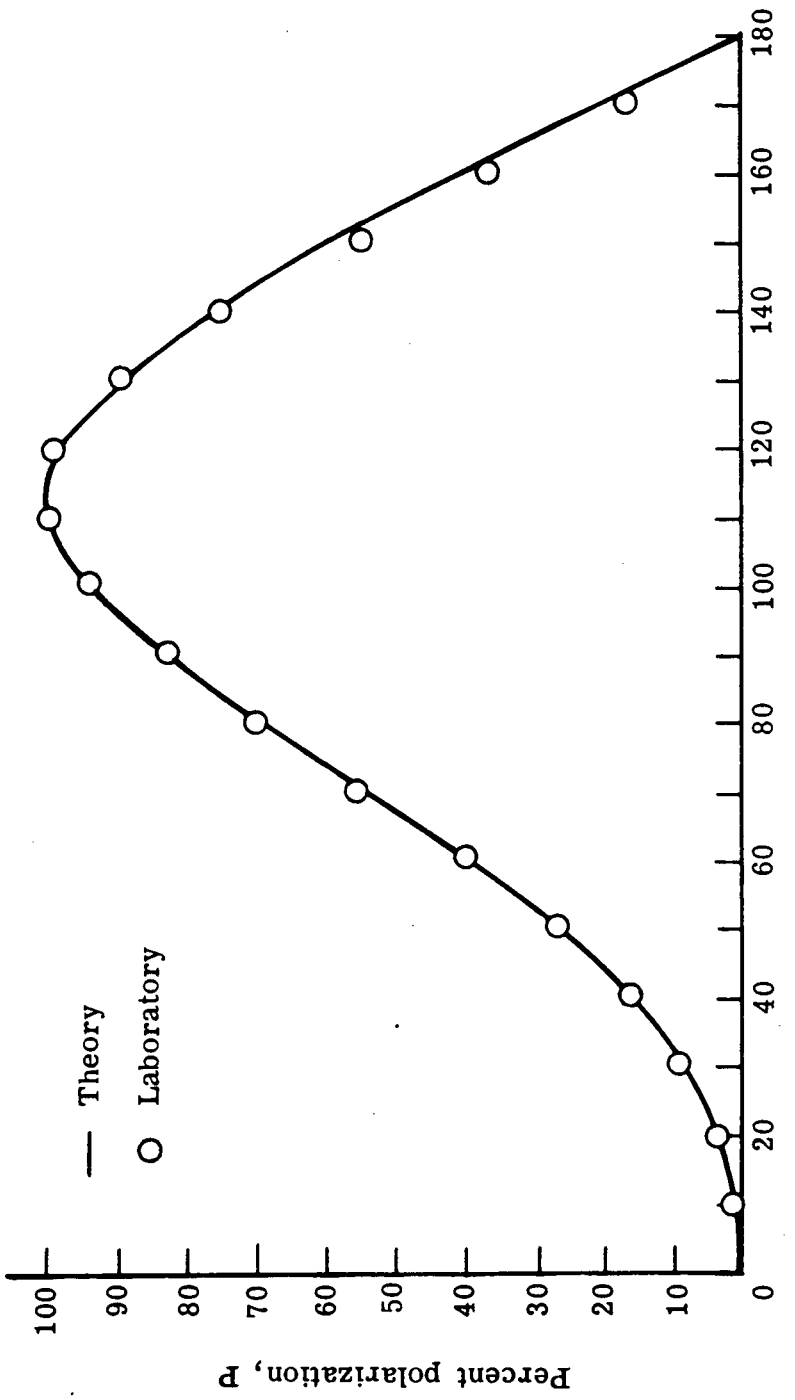

Figure 10.- Percent polarization of light specularly reflected from zinc crown glass (n = 1.52). The laboratory data represent averages of the measurements made in the ultraviolet, blue, and visual spectral bands; the typical spread in data was less than ± 2.0 percent polarization.

newtons were applied to the Echo II and PAGEOS I materials respectively producing stresses of 479 and 70 n/cm^2. These values of stress were applied because the Echo II satellite skin stress was found to have been 331 n/cm^2 (Refs. 18 and 19) during its early lifetime, and because the stress for the PAGEOS I was found to have been 52 n/cm^2 (Ref. 14).

Since the polarization properties of the Echo II material was found to be dependent upon the orientation of its surface line structure with respect to the plane of incidence (Ref. 16), the stress was applied along and perpendicular to the structure (see figure 11). This procedure was not used for the PAGEOS I material because its surface is almost optically smooth.

After the relaxation period, the percent polarization of light reflected from each test material was measured in the manner described in the polarization measurements section. The Echo II material was polarimetrically measured with the surface line structure oriented parallel and perpendicular to the plane of incidence. Unstressed samples of the materials were investigated for comparison purposes.

Surface Geometry

The effect of surface geometry upon the basic polarization properties was investigated by examining the light reflected from spherical models described in Chapter III. The light path of the measured light is illustrated in figure 12 where a 12.70-cm-diameter collimated light beam is projected upon a 12.70-cm-diameter sphere, and the light reflected in a one degree cone is measured by the detection unit 8.0

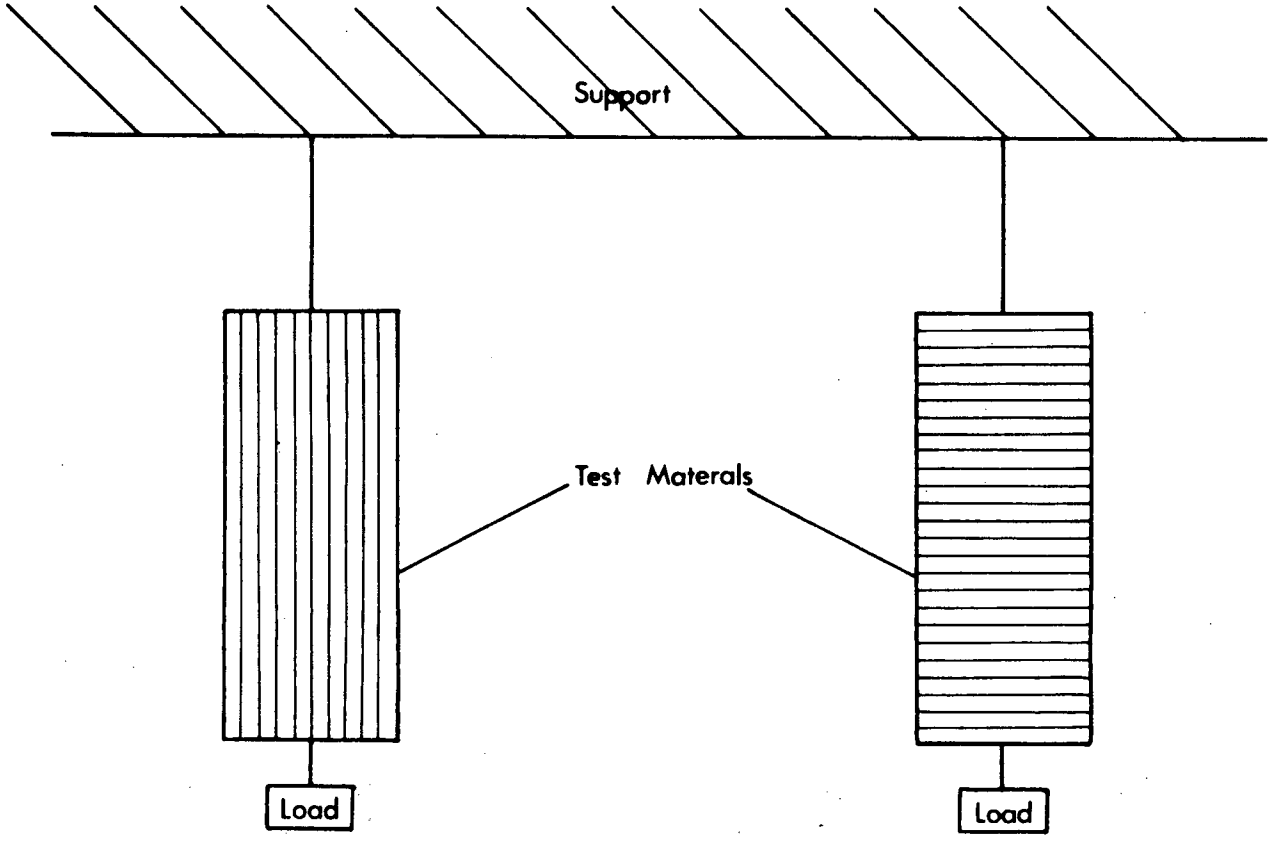

Figure 11.- Direction of stress applied to the Echo II test materials with respect to the surface line structure.

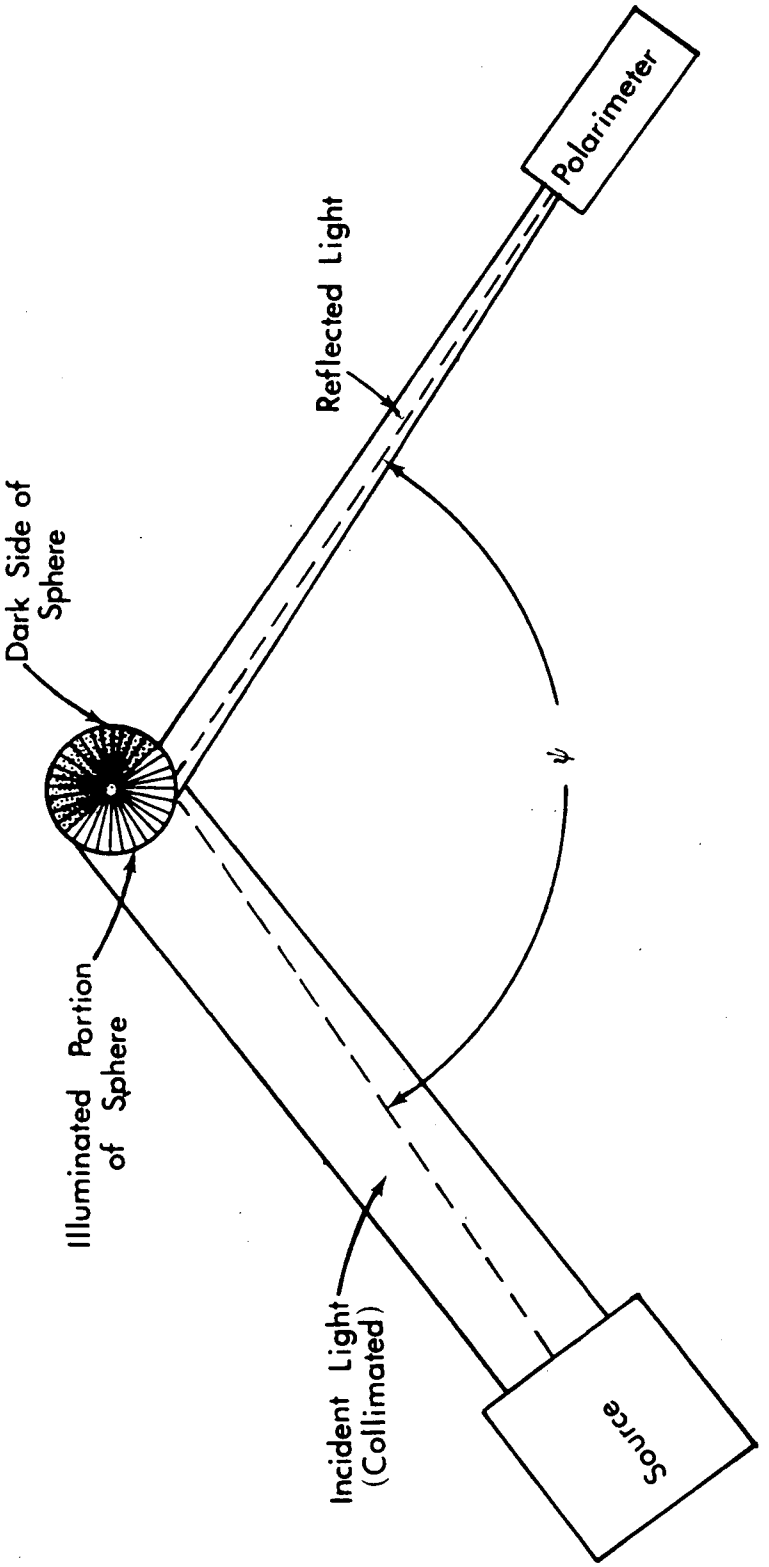

Figure 12.- Path of light reflected from test sphere.

meters away. The polarization of the light was measured with the gores of the spheres oriented parallel and perpendicular to the plane of incidence.

Vacuum Test

The effects of vacuum upon the light polarizing properties of the Echo II and its aluminum substrate materials were investigated using a 200 liter ultra high vacuum chamber. The cylindrical chamber (figure 13) is capable of producing vacuum pressures as low as 10^{-12} torr using Vac-Ion, sorption, and sublimation pumps; it has numerous quartz viewing ports. The viewing ports used were found in a plane perpendicular to the axis of symmetry for the chamber, and located on the circumference of the chamber. The source and detection units of the goniophotometer were externally mounted to the chamber at appropriate viewing ports which permitted phase angles, ψ, of 40°, 60°, 80°, 100°, 120°, and 140° to be obtained. The sample unit was located inside the chamber with its axis of rotation coinciding with the axis of symmetry for the chamber. The light path in the apparatus is given in figure 14. As depicted in the figure , a collimated light beam passes through a viewing port into the chamber, and is projected upon the test material at a preselected angle of incidence θ_1. The light, specularly reflected ($\theta_1 = \theta_1'$) from the test material at a preselected phase angle ψ, passes through another port out of the chamber to the detection unit. The percent polarization of the reflected light was determined in the manner described in the polarization measurements section.

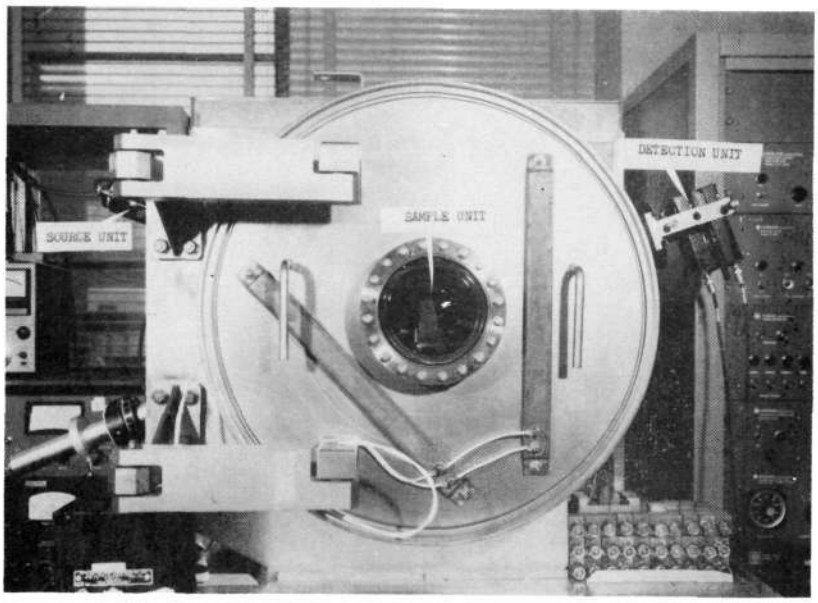

a.- Chamber closed

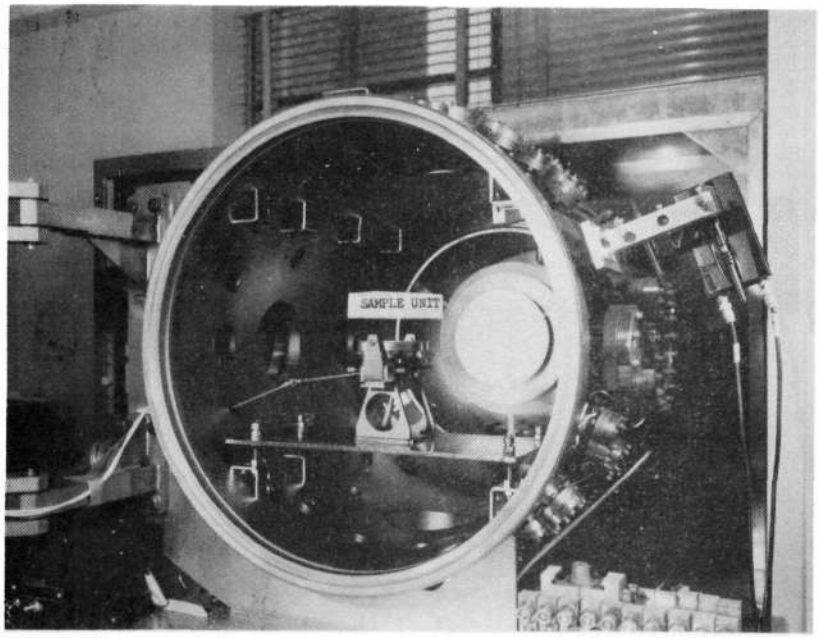

b.- Chamber open

Figure 13.- 200 liter ultra high vacuum chamber equipped with polarimeter.

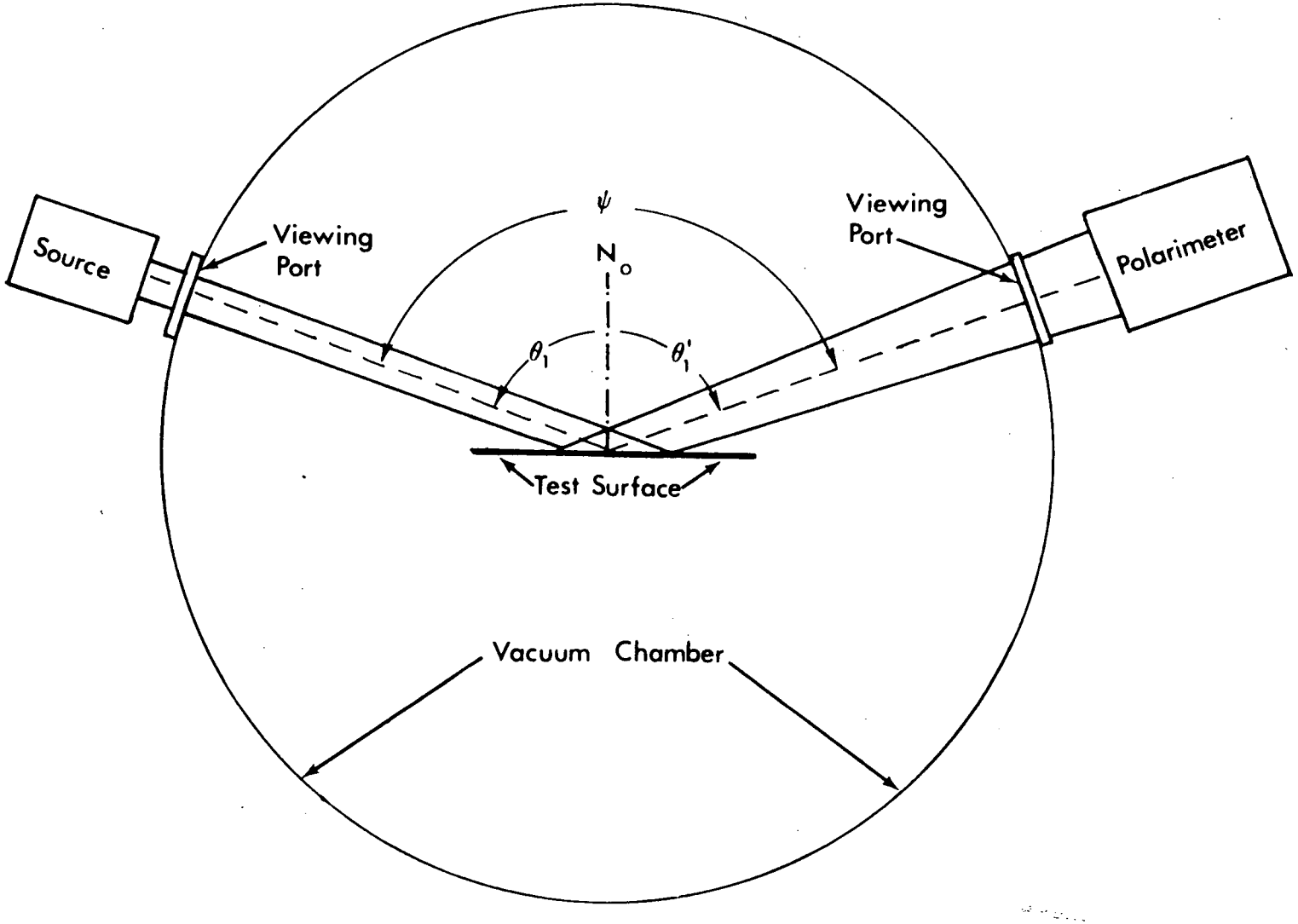

Figure 14.- Optical path of light measured in the ultra high chamber equipped with polarimeter.

Before the materials were subjected to vacuum, their light polarizing properties were determined with the materials inside the chamber at atmospheric pressure (760 torr) and room temperature (25°C) in an air atmosphere. Next, the materials were exposed to vacuum of the order of 10^{-7} torr for specified periods of time. The Echo II material was exposed to vacuum for at least 130 hours because its outgassing rate was found to stabilize after 120 hours (Ref. 13) while the aluminum substrate was exposed to vacuum for 66 hours because its outgassing rate is stable after 12 hours (Ref. 20). The primary source of outgassing for the Echo II is water vapor. After the specified times of exposure, the polarization was measured while the materials were still under vacuum. After the vacuum measurements were performed, the chamber was returned to atmosphere pressure, and the polarization of the light reflected from the materials was again measured in air and nitrogen atmospheres. The Echo II material was investigated with its surface line structure oriented parallel and perpendicular to the plane of incidence, whereas for the aluminum substrate the structure was oriented 45° to the plane of incidence. The PAGEOS I material was not investigated because the aluminum substrate measurements could be used to determine if vacuum would have any affects on its polarization properties.

CHAPTER V

SATELLITE POLARIMETRY

NASA Satellite Photometric Observatory

Using the NASA Satellite Photometric Observatory (SPO), polarimetric measurements were performed of sunlight reflected from the surfaces of the Echo II and PAGEOS I in the standard astronomical ultraviolet U, blue B, and visual V spectral bands as a function of phase angle ψ. These measurements, performed under contract, were conducted during the winters of 1967 and 1969 at Yuma, Arizona. Although the SPO and the polarimetric data reduction techniques are described in detail References 3, 4, 5, and 21, they will be briefly described in the following paragraphs.

The SPO consists of a telescope complex housed in a van on the rear of a truck (fig. 15). When the sides of the van are deplored, they form a stable observation deck for the telescope complex (figure 16). The complex consists of three auxiliary telescopes and a main telescope. The auxiliary telescopes are used to acquire and establish the tracking pattern of a satellite or star for the main telescope. The main telescope collects sunlight reflected from the satellites or starlight which is polarimetrically measured. Its primary mirror, 24 inches in diameter, has a f/4 Newtonian mode while its secondary mirror, in a Cassegrain mode provides a magnification of 5, resulting in an overall focal ratio of f/20 for the main telescope. The complex is mounted on a four axis

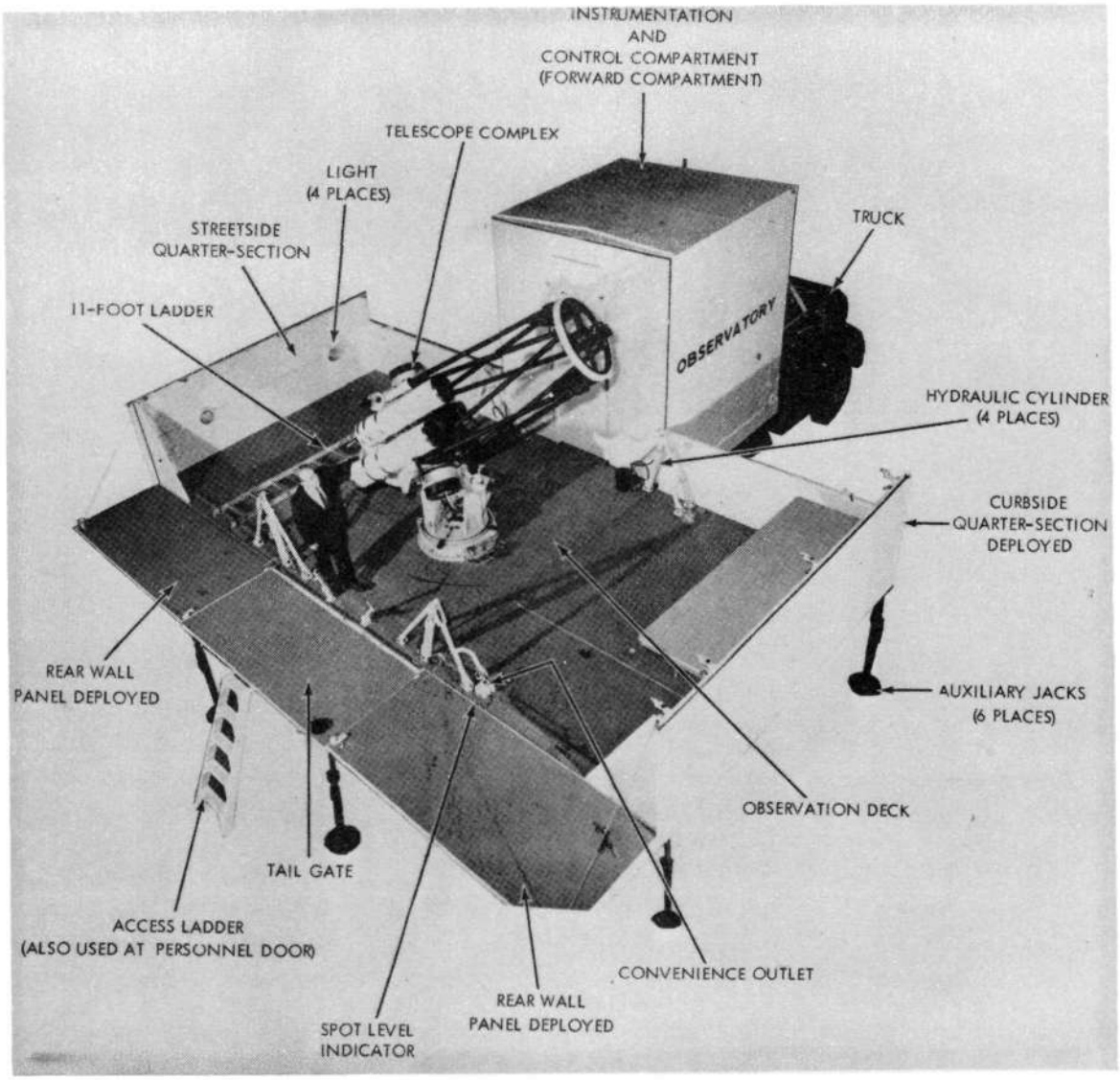

Figure 15.- NASA Satellite photometric observatory-deployed.

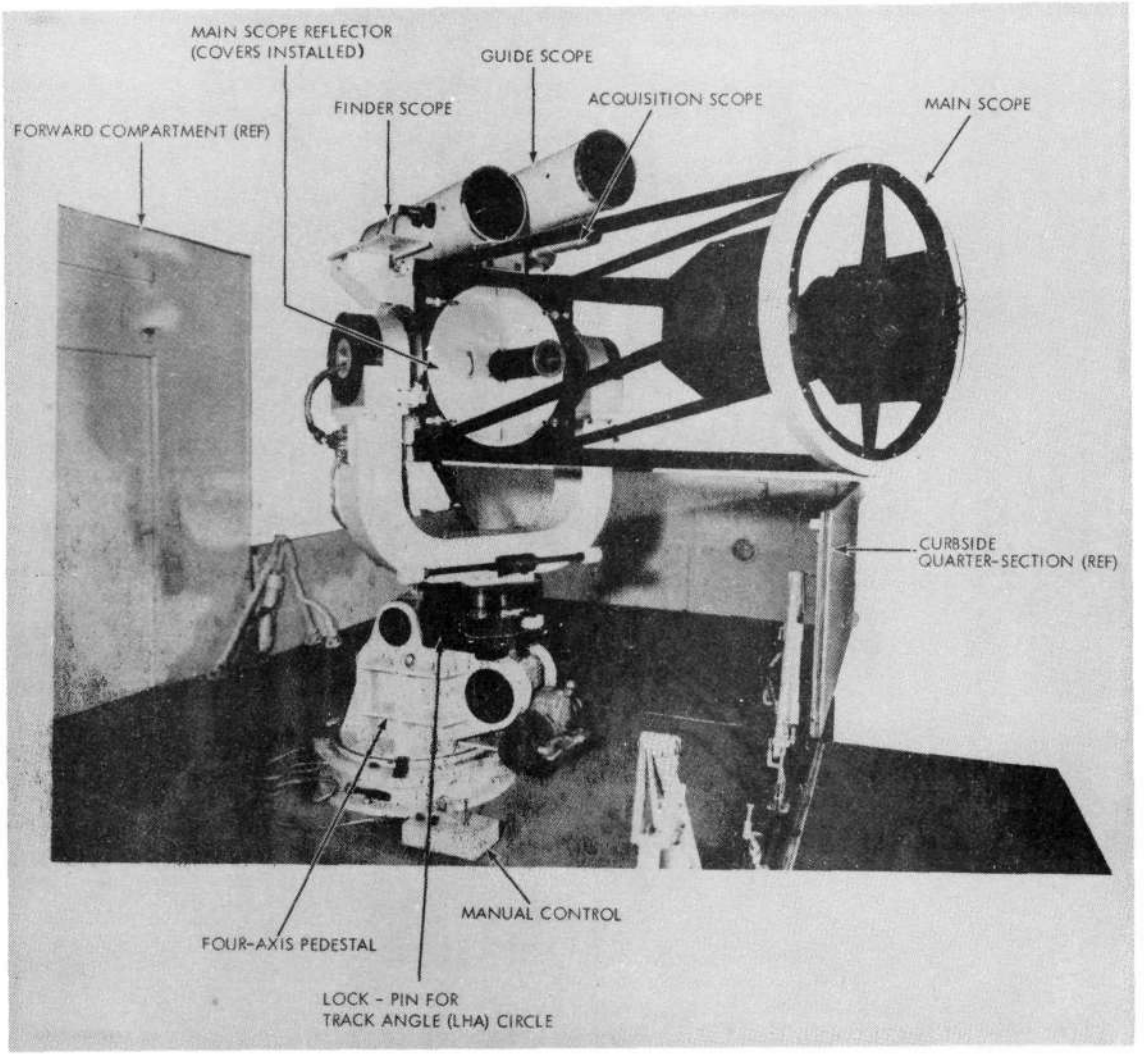

Figure 16.- Telescope complex.

pedestal especially designed for satellite tracking. Starting at the base, the pedestal has an Azimuth axis with $\pm$ 270° travel, a latitude axis with 0° to 90° travel, a polar axis with $\pm$ 180° travel, and a Declination axis with $\pm$ 45° travel.

The polarization of the collected light is measured by means of a polarimeter attached to the main telescope. The light path in the polarimeter is illustrated in figure 17 where the collected light passes through a rotating half-wave plate (rotated in ten steps of 36° increments), field stop, and Wollaston prism. Upon emerging from the prism, the light is separated into two orthogonal components I_1 and I_2. The orthogonal components pass through lenses and a depolarizer, and are reflected at 45° by silvered mirrors. The reflected components, then, pass through color filters, and finally are sensed by two photomultipler tubes. When the light was polarized, the resulting photovoltage v_1 and v_2 (corresponding to I_1 and I_2)varied as the $\sin^2(\eta_1-2\beta)$ and $\cos^2(\eta_1-2\beta)$ where β is the angle between the optical axis of the half-wave plate and a reference axis (declination axis) on the telescope, and η_1 is the angle between the plane of polarization of the polarized light and a reference axis on the telescope. The angles β and η_1 are illustrated in figure 18. Also, an example of the variation of v_1 and v_2 with β is given in figure 19. The data points represent the photovoltages averaged for approximately two second periods at each position of the half-wave plate.

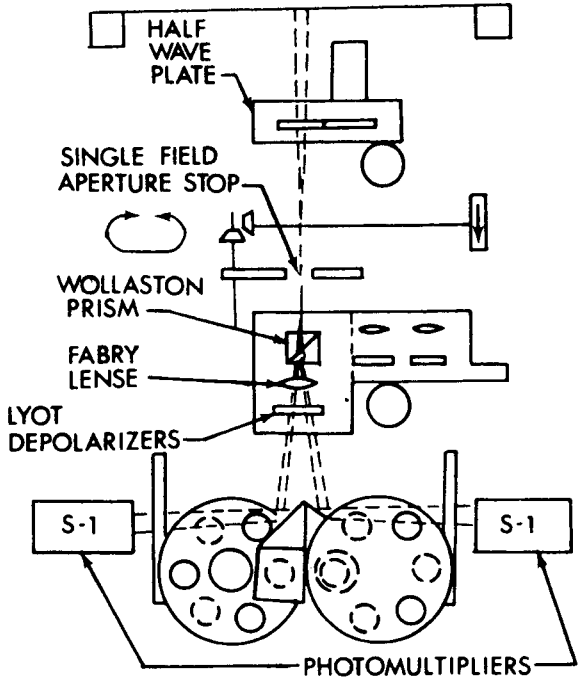

Figure 17.- Light path in polarimeter attached to the main telescope.

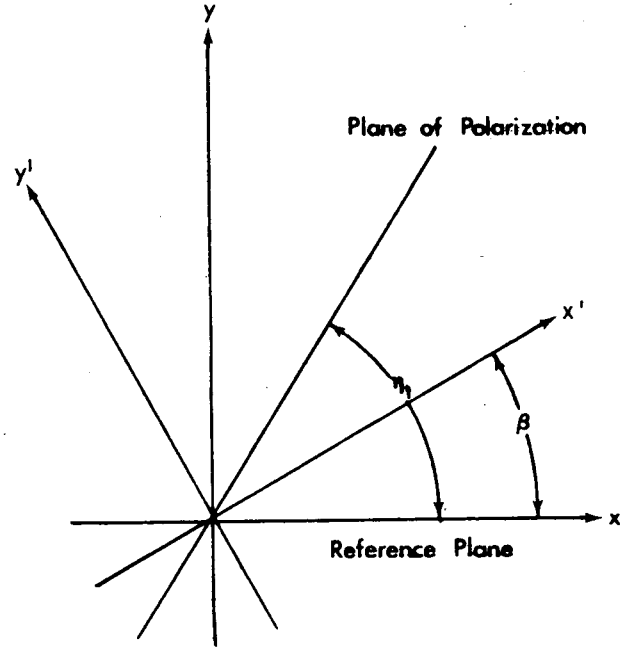

Figure 18.- Illustration of the angles β and η_1. The x' and y' axes indicate directions along and perpendicular to the active axis of the half-wave plate with the x and y axes denote directions along and perpendicular to the active axis of the Wollasten prism.

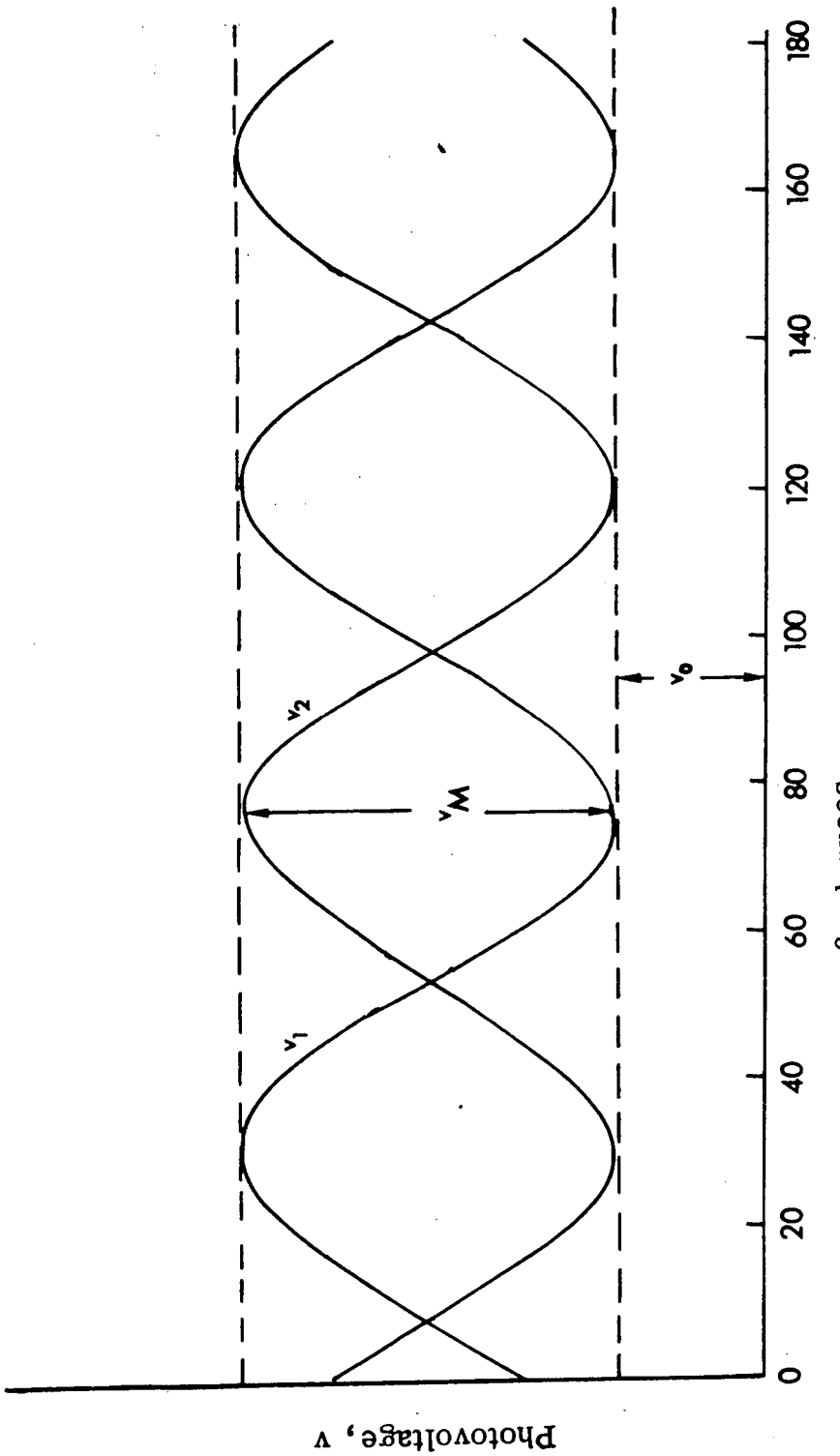

Figure 19.- Example of the variation of v_1 and v_2 (corresponding to I_1 and I_2) with β, assuming η_1 to be equal to 60. v_M and v_o correspond to the polarized, I_p, and the unpolarized, I_u, components of light.

Polarization Determination

The degree of polarization P of the collected light was determined using the following data reduction equation

$$\frac{I_{y_i} - I_{x_i}}{I_{y_i} + I_{x_i}} = P \cos(2\eta - 4\beta) \tag{29}$$

Equation (29) is taken from Reference 3.

Before the true degree of polarization of reflected sunlight was determined, the instrumental and sky background ($\psi > 120°$) polarization were determined and compensated for in the satellite intensities. The instrumental polarization was determined using a star calibration method. In the method, stars found in the Alfred, Behr Catalog (Ref. 21) were polarimetrically measured along the satellite path, and the resulting values of P were compared to the published values for the stars. If differences were observed, the adjusted values of I_2 compensating for instrument polarizations, were determined by fitting a quadratic equation to the I_1/I_2 ratios for each nonpolarized star and by multiplying the polarized star and satellite values of I_2 by the resulting best fit quadratic equation. That is

$$I_{2A} = I_2 f(\beta) = I_2(Z_1 + Z_2\beta + Z_3\beta^2) \tag{30}$$

where Z_1, Z_2, Z_3 are the quadratic coefficients.

Next, the intensity of the sky background was measured along the satellite path at high phase angles ($\psi > 120°$). These values were

vectorially subtracted from the I_1 and I_{2A} values, yielding the true values of I_{y_i} and I_{x_i} for the satellites.

Next, the I_{y_i} and I_{x_i} values obtained for each particular phase angle were substituted into the left side of eq. (29), and the resulting values of A and B were used to determine P and η.

$$A = \frac{(\sum_i Y_i \cos 4\beta_i)(\sum_i \sin^2 4\beta_i) - (\sum_i \sin 4\beta_i \cos 4\beta_i)(\sum_i Y_i \sin 4\beta_i)}{(\sum_i \cos^2 4\beta_i)(\sum_i \sin^2 4\beta_i) - (\sum_i \sin 4\beta_i \cos 4\beta_i)^2} \tag{31}$$

$$B = \frac{(\sum_i \cos^2 4\beta_i)(\sum_i Y_i \sin 4\beta_i) - (\sum_i Y_i \cos 4\beta_i)(\sum_i \cos 4\beta_i \sin 4\beta_i)}{(\sum_i \cos^2 4\beta_i)(\sum_i \sin^2 4\beta_i) - (\sum_i \sin 4\beta_i \cos 4\beta_i)^2} \tag{32}$$

where $$Y_i = \frac{I_{y_i} - I_{x_i}}{I_{y_i} + I_{x_i}} \tag{33}$$

$$P = \sqrt{A^2 + B^2} \tag{34}$$

$$\eta_1 = 1/2 \tan^{-1} \left(\frac{B}{A}\right) \tag{35}$$

Finally, the true angle of polarization is given by

$$\eta = \eta_1 - b \tag{36}$$

where b is the angle between the active axis of the Wollaston prism (declination axis of telescope) and the plane of incidence. See Appendix B for the determination of the angle b.

CHAPTER VI

RESULTS AND DISCUSSIONS

The percent polarization P of light reflected in the specular direction from test materials is presented as a function of phase angle ψ in the ultraviolet, blue, and visual spectral bands. The laboratory measurements are presented in figures (20) through (26) while the satellite polarization measurements of the PAGEOS and the Echo II are given in figures (27) through (30). The bars in each figure represent the typical data spread from the average or the probable error.

Laboratory

Echo II Material.- The effects of skin strain, surface geometry, and vacuum upon the light polarizing properties of the Echo II material are examined in this section. Because the polarization of light reflected from the Echo II is dependent upon the orientation of its surface line structure with respect to the plane of incidence, the measurements were performed with the structure oriented perpendicular and parallel to the plane of incidence. These respective surface orientations represent positions where the polarization has been observed to exhibit maximum and minimum values for phase angles greater than 100° (Ref. 16). For convenience, P_s and P_p will respectively refer to the percent polarization measured with the structure oriented perpendicular and parallel to the plane of incidence while $\bar{P}$ will refer to the average of P_s and P_p, or polarization measurements obtained with the structure oriented at 45°.

In figure (20), the effect of strain upon the light polarizing properties of the Echo II material is examined where the average, percent polarization, $\bar{P}$, $(P_p + P_p)/2$, for the flat, unstressed surface is compared to that for the surfaces which have been subjected to uniaxial stress of approximately 479 n/cm^2. Although the comparison reveals slight differences in the polarization at phase angles ψ greater than 120^o, the differences are not outside of the experimental error ($\pm$ 2.0 percent polarization), and hence stress (less than 479 n/cm^2) can not be considered as a mechanism capable of significantly affecting the polarization.

Also, in figure (20), the average polarization $\bar{P}$ of light reflected from a sphere, constructed of the Echo II material, is compared to that for the flat surfaces. The sphere is found to polarize the light considerably less than the flat surfaces. The polarization for the sphere was lower because it reflected a significant component of diffuse light (in the specular direction) which added to the specular light component reduced the polarization, as predicted by equation (24).

$$P = \frac{\rho_s - \rho_p}{\rho_s + \rho_p + 8/3(\gamma_s + \gamma_p)F(\psi)} \qquad (24)$$

In the case of the flat surface, the polarization was not affected by the diffuse light since its magnitude was much less than that for the specularly reflected light, in other words

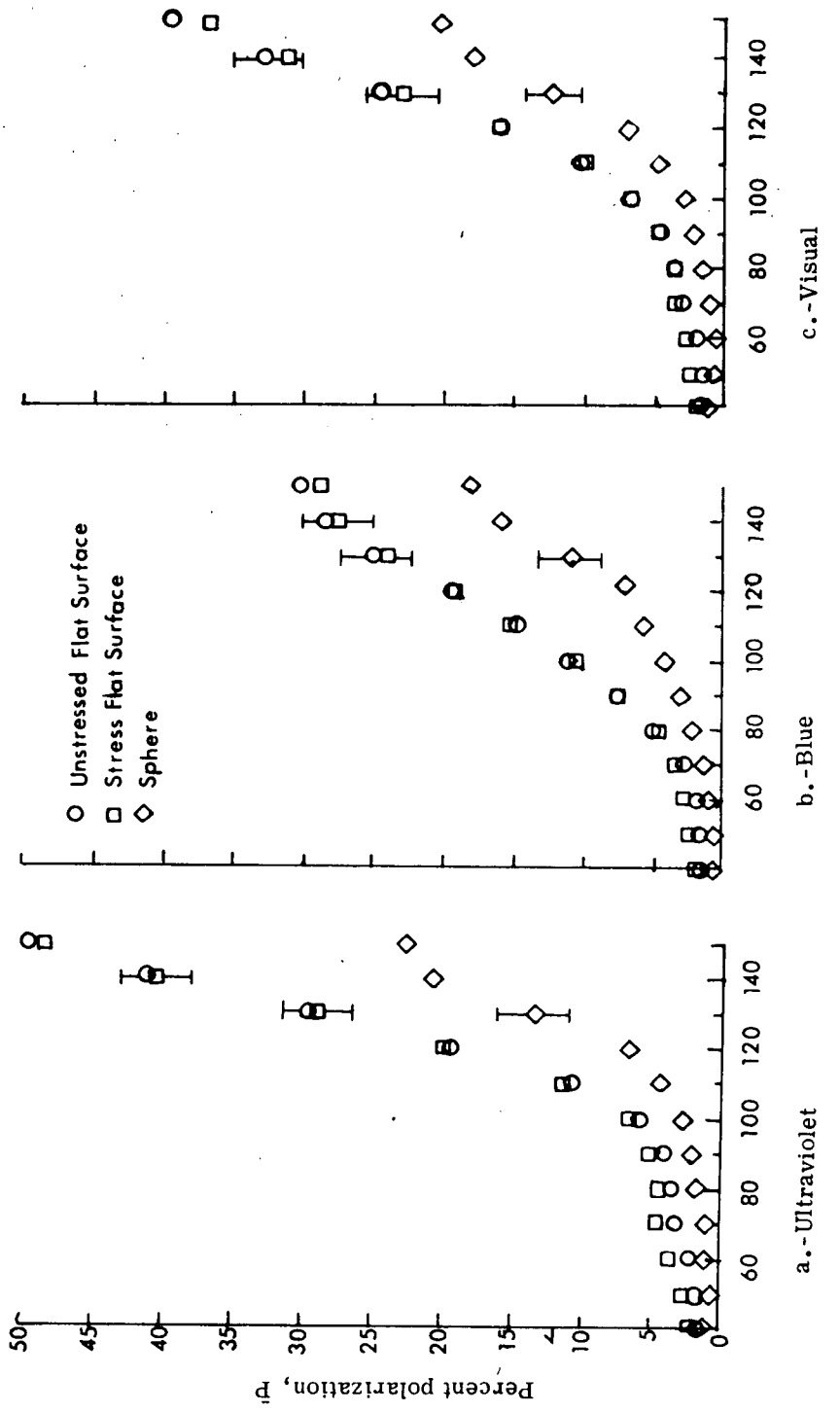

Figure 20.- Effects of strain and surface geometry upon the light polarizing properties of Echo II test surface.

$$(\gamma_s + \gamma_p)\Delta\theta_1' << \rho_s + \rho_p \tag{37}$$

where

$$\Delta\theta_1' < 10^{-3} \text{ radians} \tag{38}$$

Thus, equation (17) describing the polarization for the flat surface

$$P = \frac{\rho_s - \rho_p}{\rho_s + \rho_p + (\gamma_s + \gamma_p)\Delta\theta_1'} \tag{17}$$

could be approximated by

$$P = \frac{\rho_s - \rho_p}{\rho_s + \rho_p} \tag{39}$$

Comparing equations (24) and (39), it can be seen that the polarization for the sphere should have been lower than that for the flat surface. Although the sphere polarized the incident light less than the flat surfaces, it polarized the light in increasing amounts in the blue, visual, and ultraviolet spectral bands, the same as the flat surfaces did.

Generally, the polarization of light reflected from a surface decreases as the phase angle approaches 0° such as in the case for the flat Echo II surfaces. Looking at figure (20), the polarization for the Echo II sphere appears to have decreased to minimum values in the 40° to 60° phase angle range, and thereafter to have increased as the phase angle approached 0°. This unusual trend was probably caused by

the light diffusely reflected from the sphere having a polarization component greater than that for the specularly reflected light for phase angles less than 50°, and a plane of polarization essentially parallel to the plane of incidence (angle of polarization η approximately equal to 0°). Looking at figure (21), η for the sphere is found to be less 45° and decreasing to 0° for phase angles less than 50°. This indicates that the plane of polarization was essentially parallel to the plane of incidence. Considering the trends for $\bar{P}$ and η and examining equations (22) and (25), it appears reasonable to assume that the light diffusely reflected from the Echo II sphere was polarized in the plane of incidence, and to a greater degree than the specularly reflected light.

Notice how η for the aluminum substrate sphere, shown in figure (21), is essentially 90° for the entire phase angle range, indicating that the plane of polarization was oriented perpendicular to the incidence plane. Since η varied with phase angle differently for the Echo II sphere than the aluminum sphere, it should be possible to determine if the Echo II satellite had a reflecting surface of alodine on aluminum. Although the data is not shown, the spheres constructed of the Echo II and aluminum substrate materials polarized the incidence light the greatest with their surface line structures oriented perpendicular to the plane of incidence, and the least with the structures oriented parallel for phase angles greater than 100°. This is the reverse of the trend observed for the flat surfaces (Ref. 16). The

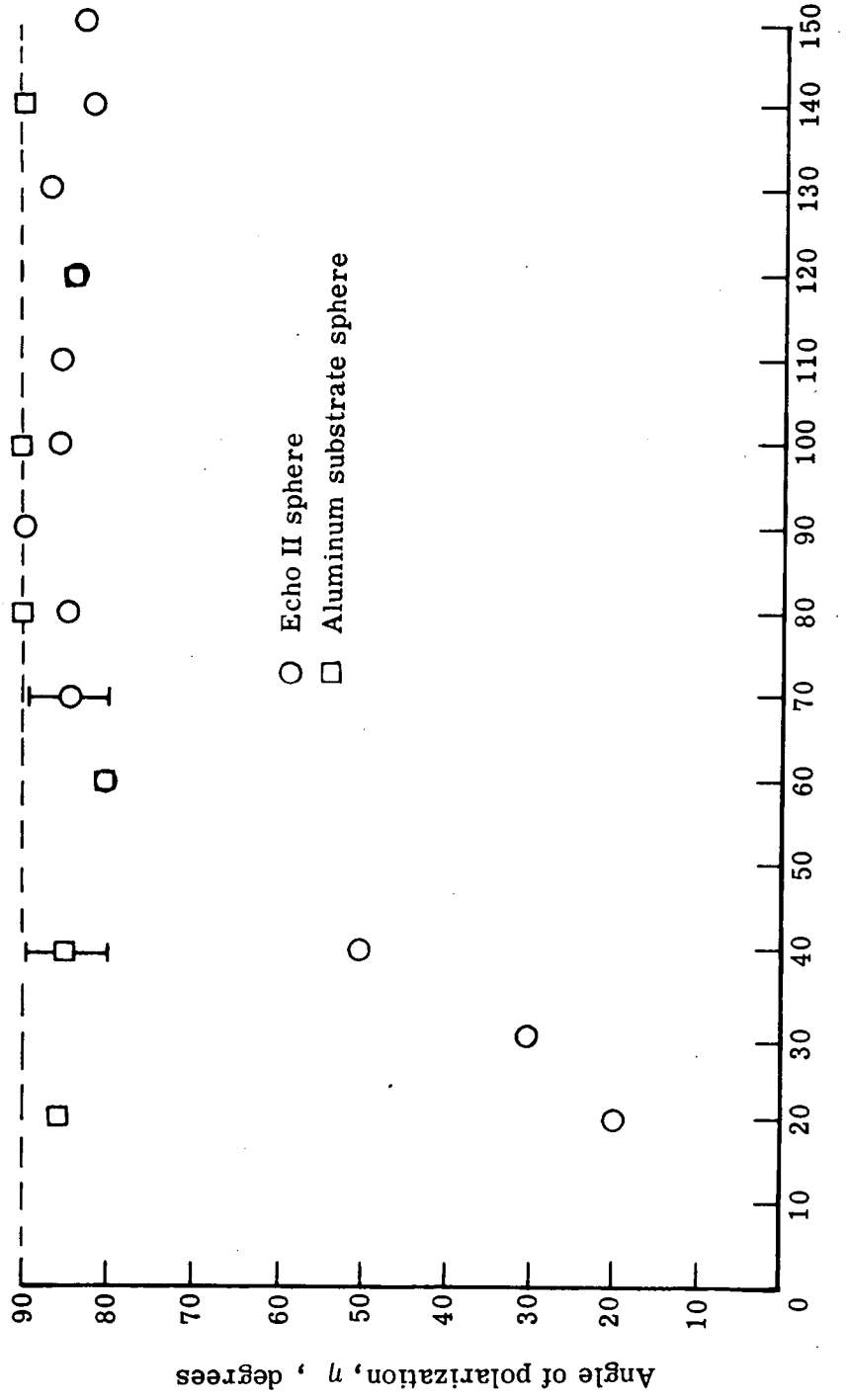

Figure 21.- Variation of the angle of polarization η with the phase angle ψ for the Echo II and aluminum substrate spheres.

trend for the spheres was expected when one considers the facts that the spheres reflect more specular light with their structures oriented perpendicular to the plane of incidence than with their structures parallel, and that the magnitude of the diffusely reflected light is independent of the orientation of their structures.

In figures (22) through (25), the effect of vacuum of the order of 10^{-6} torr upon the polarimetric properties of the Echo II material is examined. The symbols P_s and P_p refer to polarization measurements obtained with the surface line structure of the test surface oriented perpendicular and parallel to the plane of incidence while $\bar{P}$ refers to the average polarization , $(P_s + P_p)/2$.

In figure (22), the average polarization $\bar{P}$ of light reflected from the Echo II material obtained in air at room temperatures and atmospheric pressure is compared to that obtained in vacuum (10^{-6} torr) at room temperatures. The comparison revealed that the material was altered by vacuum exposure to the extent of enhancing its light polarizing properties in the blue spectral band while diminishing them in the visual and ultraviolet bands. It is believed that the observed changes were probably caused by the outgassing of water vapor from the surface (Ref. 13), resulting in changes in the optical properties of the surface. To verify this conclusion, the polarization was measured in air (containing water vapor) and in nitrogen (containing no water vapor) at atmospheric pressure and room temperatures after vacuum exposure. In figure (23), the polarization measured in air (after vacuum exposure) is compared to that measured in vacuum where it is found

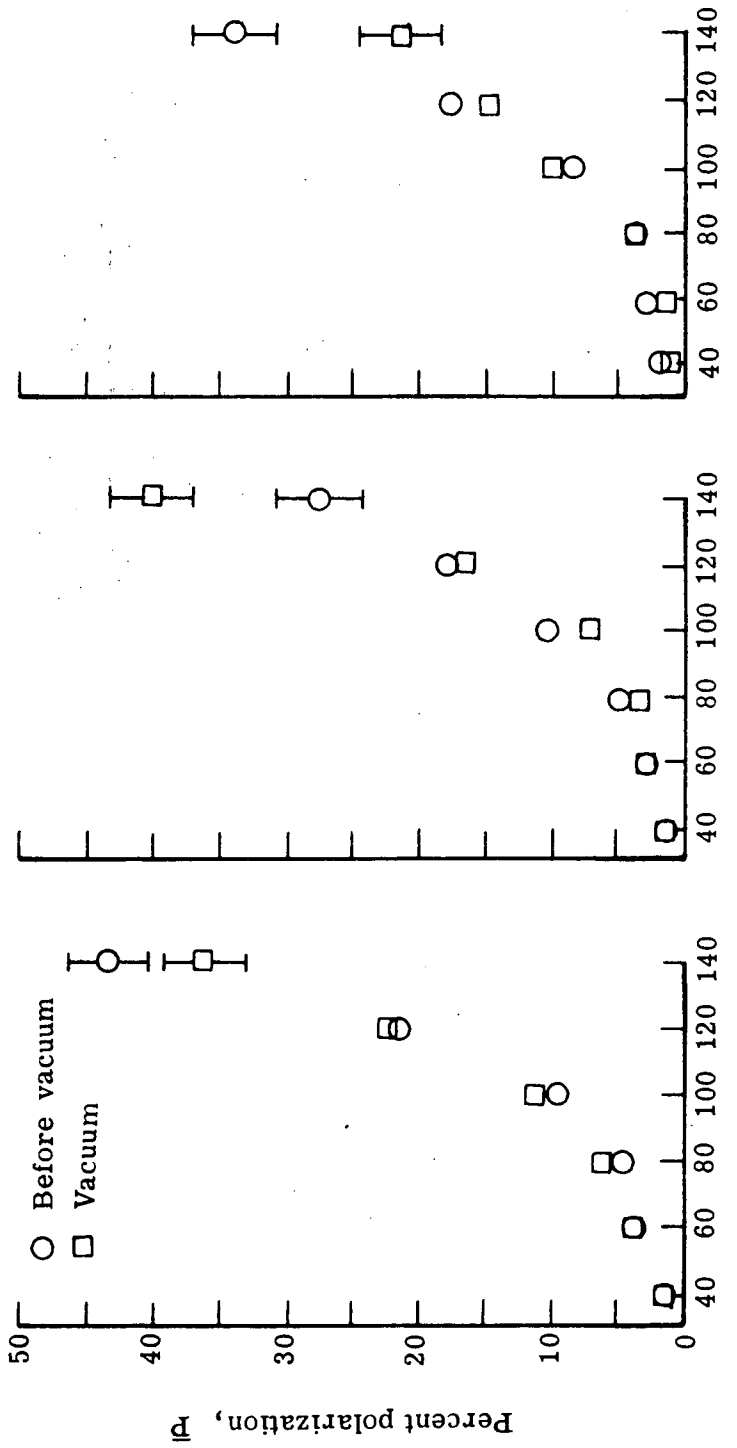

Figure 22.- Average percent polarization $\bar{P}$ for the Echo II surface before vacuum exposure and after over 130 hours of vacuum (10^{-6} torr).

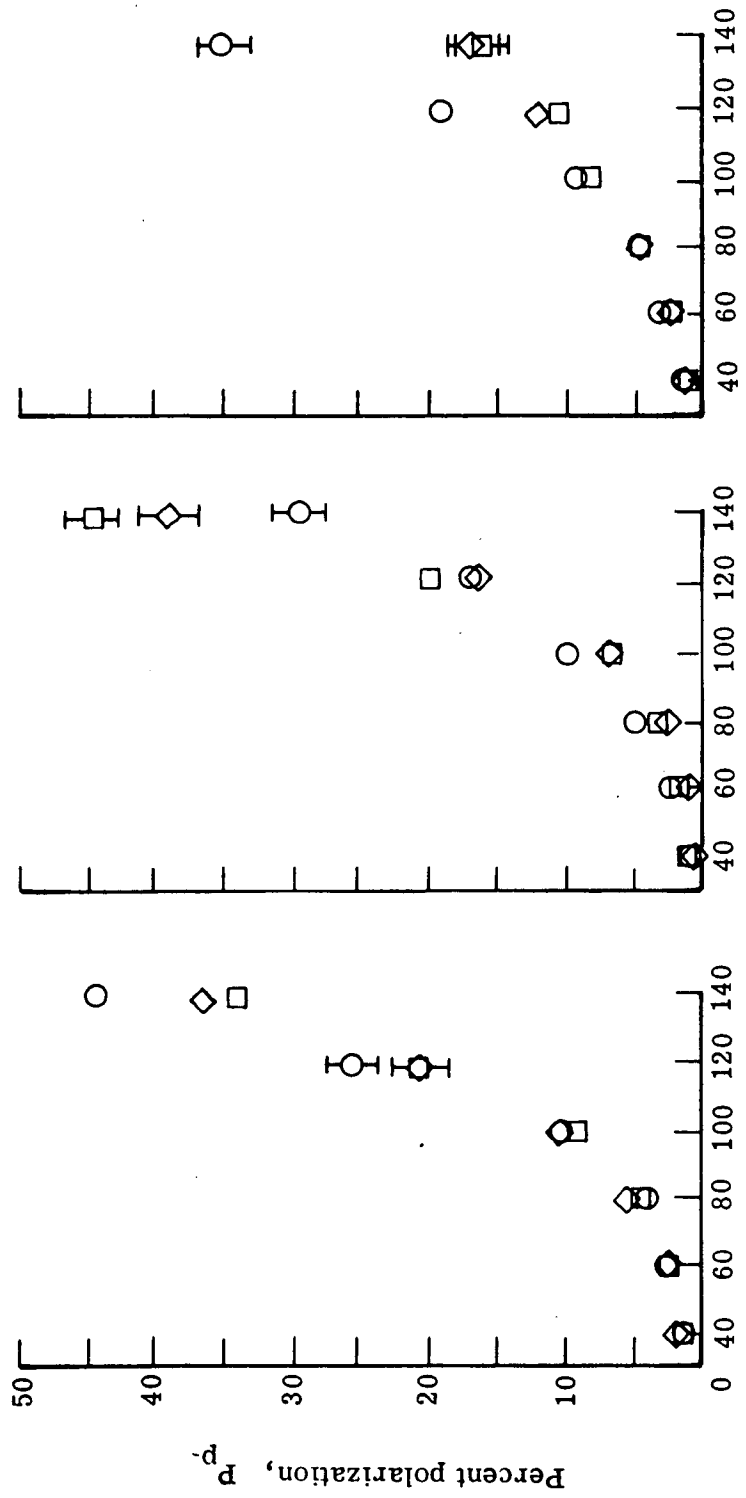

Figure 23.- Percent polarization P_p for the Echo II surface plotted against phase angle ψ in the ultraviolet, blue, and visual spectral bands. Test environments: ○ air (760 torr, 25°C) before vacuum, □ 148 hours of vacuum (10^{-6} torr, 25°C), and ◇ 24 hours of air (760 torr, 25°C) after vacuum.

to be slightly increasing in the ultraviolet and visual spectral bands, and decreasing in the blue band toward the polarization values measured in air before vacuum exposure, suggesting the absorption of water. Whereas, the polarization measured in nitrogen (after vacuum exposure) essentially remained the same as that measured in vacuum, see figure (24). These results obtained in air and nitrogen tend to support the idea that the observed changes for the Echo II material in vacuum were primarily caused by water losses altering the material's optical properties.

$\bar{P}$ for the aluminum-foil substrate was measured in air and vacuum to determine whether the Echo II material's polarization changes were caused by the alodine coating or the substrate experiencing changes in its optical properties. In figure (25), the polarization data for the substrate indicate that vacuum exposure had no significant effect upon its polarization. This indicates that the alodine coating had changed in vacuum.

It is interesting to note that the Echo II material polarized the incident light in increasing amounts in the following order of spectral bands: visual, ultraviolet, and blue while it was in vacuum. This is different from the order of blue, visual, and ultraviolet observed for the material in air.

PAGEOS I material. - In figure (26), the polarization data from a flat, unstressed sample of the PAGEOS I material are compared to those for a flat sample subjected to uniaxial stress of approximately 70 n/cm^2. The slight differences in polarization are not outside of the

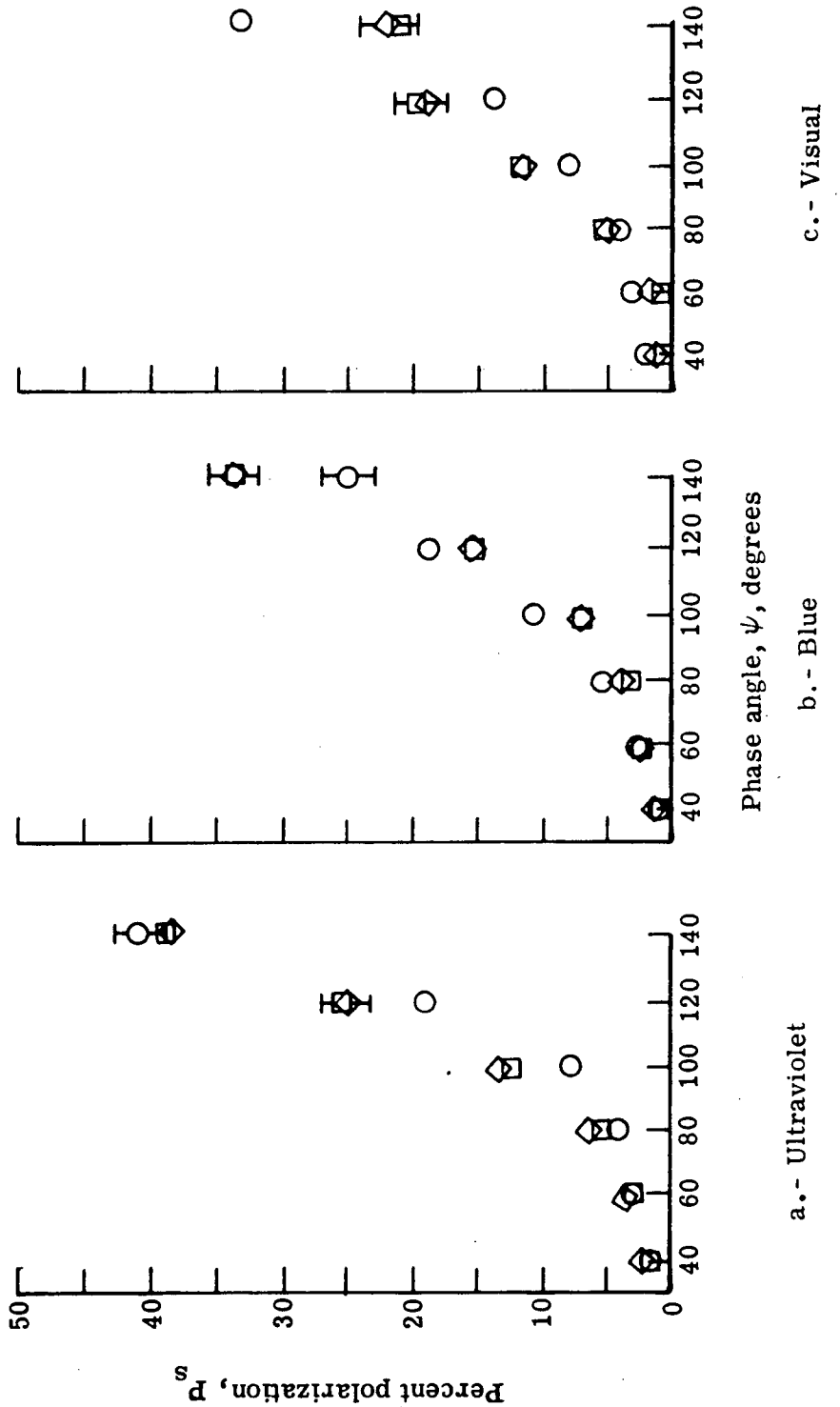

Figure 24.- Percent polarization P_s for the Echo II surface plotted against phase angle ψ in the ultraviolet, blue, and visual spectral bands. Test environment: ○ air (760 torr, 25°C) before vacuum, □ 138 hours of vacuum (10^{-6} torr, 25°C), and ◇ 24 hours of nitrogen. (760 torr, 25°C) after vacuum.

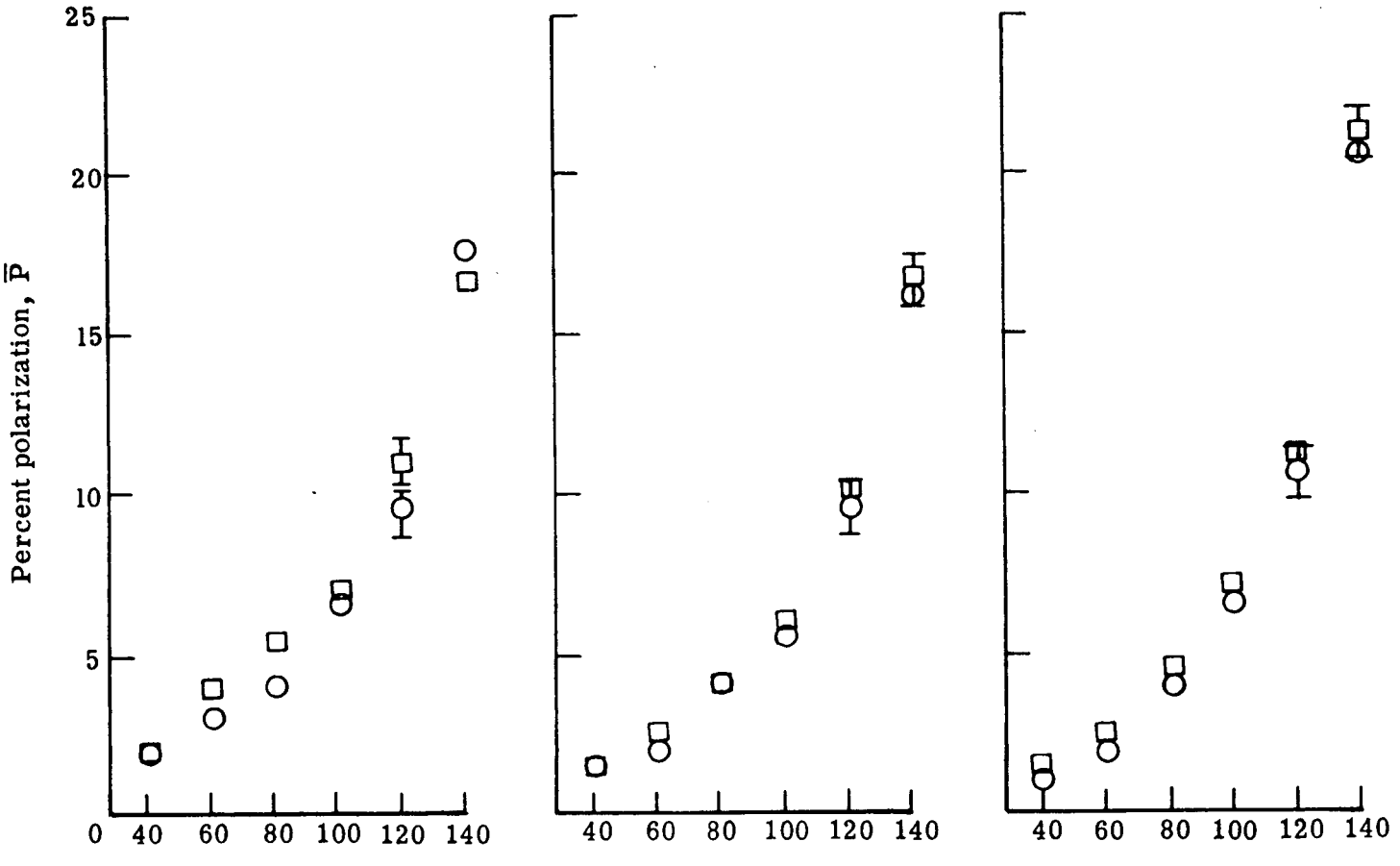

Figure 25.- Polarization $\bar{P}$ of aluminum substrate in air and vacuum environments with its surface line structure oriented 45° to the plane of incidence. Test environment: ○ air (760 torr, 25°C) before vacuum exposure, and □ vacuum exposure (10^{-6} torr, 25°C) after 66 hours.

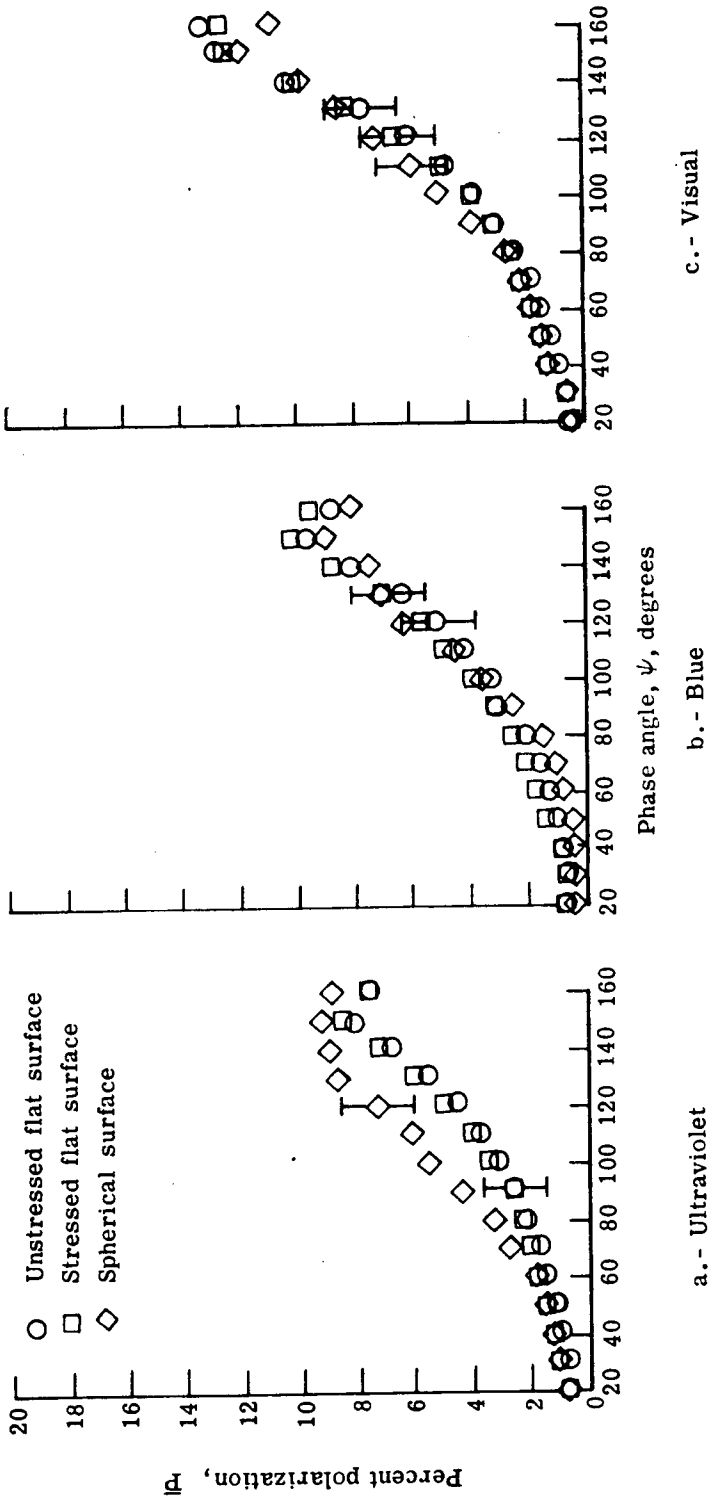

Figure 26.- Effects of strain and surface geometry upon the light polarizing properties of the PAGEOS I test surface.

experimental error, and thus are not considered to be significant, indicating that prestressing the material should not alter its basic polarization properties. The data indicates that the PAGEOS I material essentially polarized the light in increasing amounts in the ultraviolet, blue, and visual spectral bands.

Also, in figure (26), the polarization data for a sphere made of the PAGEOS I material are compared to those for the flat surfaces. The comparison indicates that the sphere polarized the incident light the same as the flat surfaces in the blue and visual bands. However, in the ultraviolet band, the comparison show significant differences. The reason for this trend is unexplained at this time.

The effect of vacuum upon the light polarizing properties of the PAGEOS I material was not explored because the vacuum-air investigation of the Echo II aluminum substrate material (Figure 25) indicated that the polarization properties of aluminum would not be discernibly altered by vacuum.

Satellites

Echo II Satellite. - The polarization measurements of the sunlight reflected from the surface of the Echo II Satellite are given in figures (27) through (29). Comparing the satellite measurements to the laboratory ones, certain features of the data can be noted. Looking at figure (27), the 1967 satellite data appears to have reached a minimum in the 40° to 60° phase angle range, and thereafter to have increased as the phase

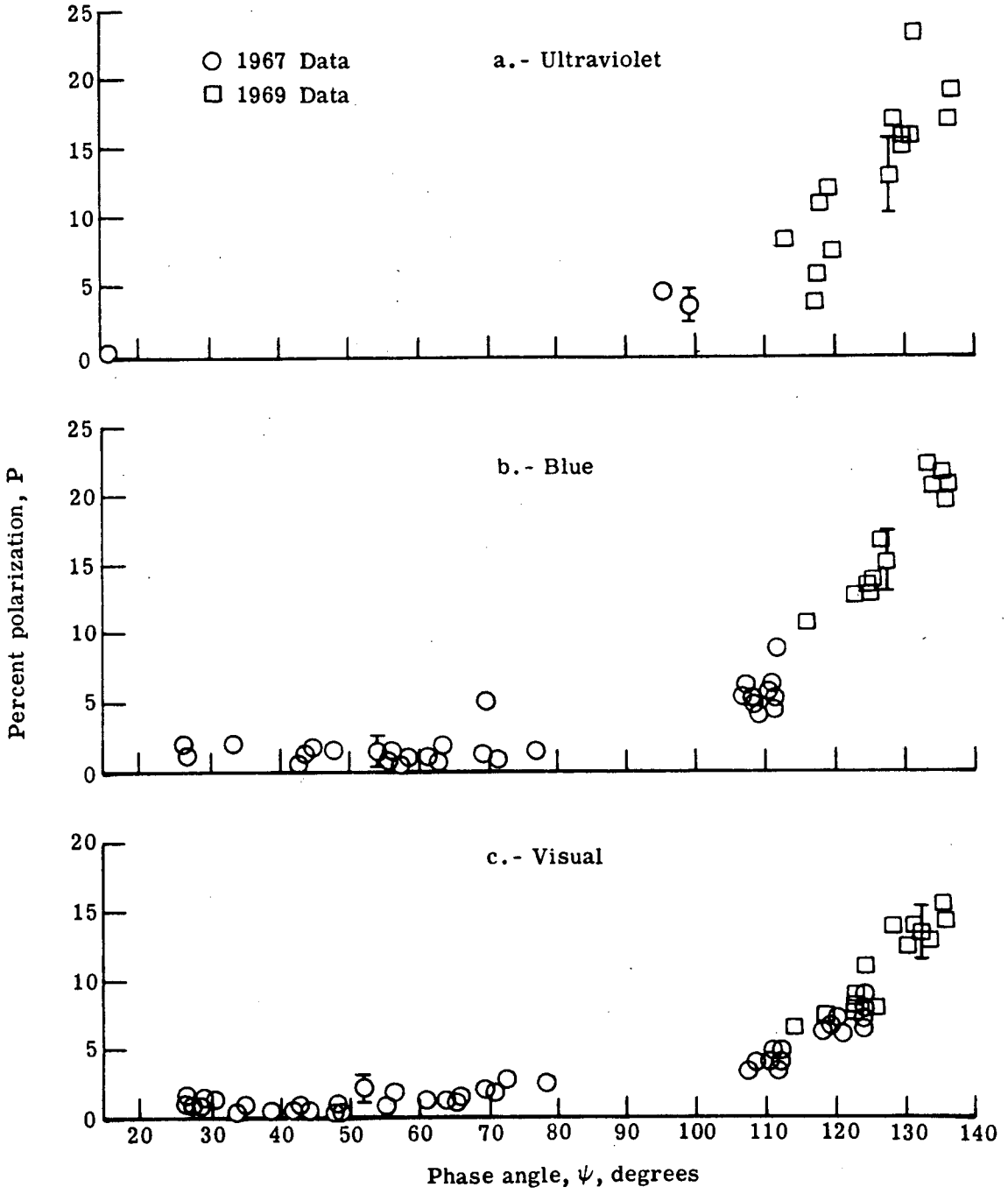

Figure 27.- 1967 and 1969 polarimetric measurements of the Echo II Satellite, obtained using the NASA Satellite Photometric Observatory.

angle approached 0°. This trend was observed in the laboratory for the sphere constructed of the Echo II material. As it was pointed out earlier in this chapter, the trend was caused by the diffusely reflected light having a larger polarization component than the specularly reflected light, and having a plane of polarization parallel to the plane of incidence. In figure (28), the plot of the angle of polarization η against ψ obtained in the visual band data supports the explanation for the above trend since η is found to be decreasing to 0°. The trend for η indicates a reflecting surface of alodine for the Echo II satellite.

The spectral polarization properties of the satellite could not be deduced in 1967 due to the lack of data points at phase angles above 110°. In 1969, this problem was resolved by obtaining measurements at the higher phase angles. The 1969 data, shown in figure (27), revealed that the satellite spectrally polarized the sunlight in increasing amounts in the visual, ultraviolet, and blue bands. This is the manner in which the Echo II material was found to polarize the light in laboratory vacuum (see figure (23)). It should be noted that the material was found to polarize the light in laboratory when exposed to air the greatest in the ultraviolet and the least in the blue which is different from the manner in which the satellite polarized the incident sunlight. This indicates that the surface of the satellite had experienced changes, mostly due to the outgassing of water vapor, in its optical surface properties as a result of exposure to space vacuum.

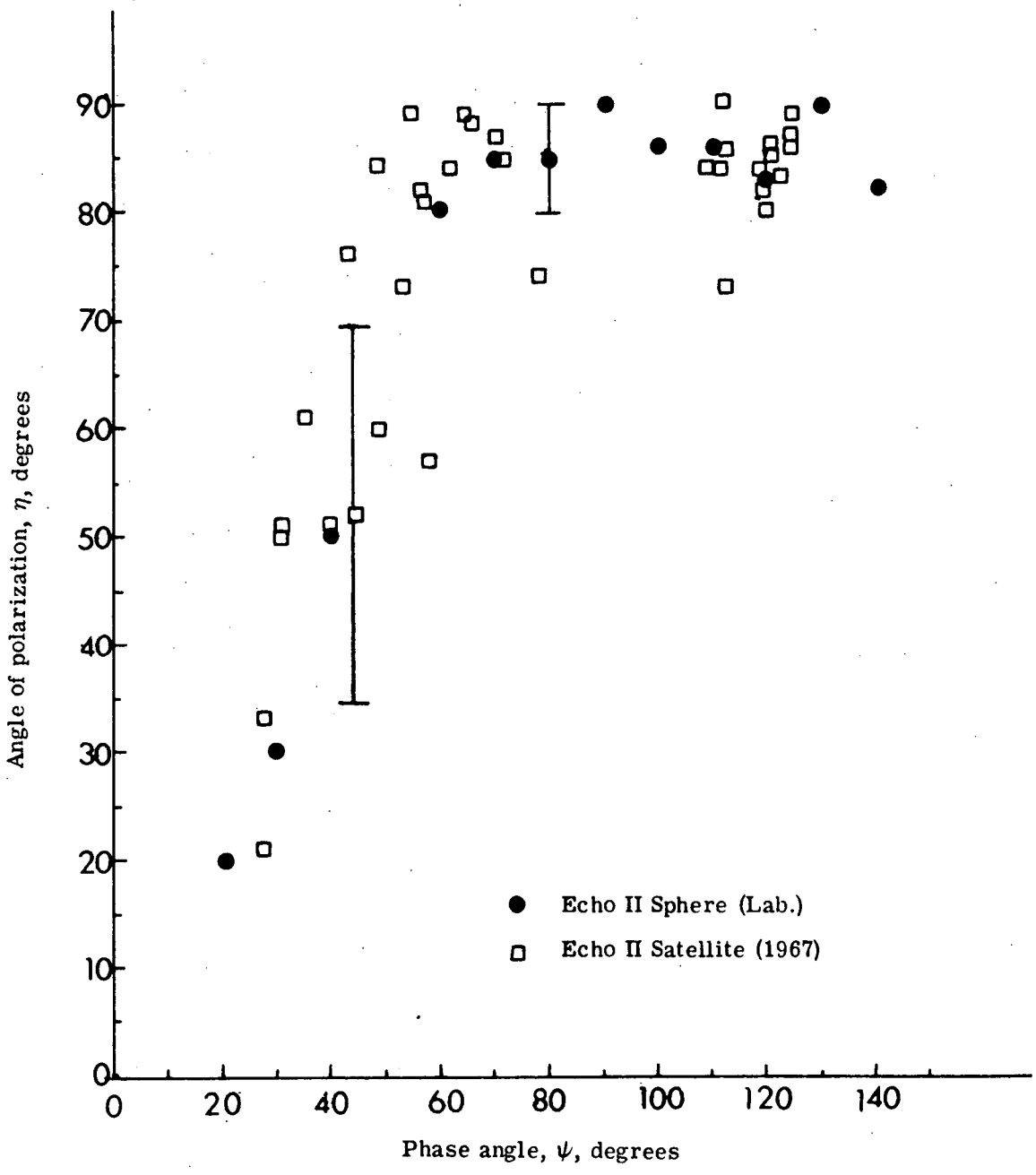

Figure 28.- Variation of the angle of polarization η with phase angle ψ for sunlight reflected from the Echo II satellite in the visual spectral band.

Looking at figure (29), it can be seen that the satellite polarized the incident sunlight considerably less than the flat Echo II material would have. The differences in the polarization were expected considering equations (39) and (24) which describe the polarization for a flat surface and a sphere.

Comparing the satellite data and the laboratory data for the Echo II sphere, the data for the sphere appear to be lower in the ultraviolet and blue, and slightly higher in the visual than the satellite data. Correcting for the effect of vacuum upon the Echo II polarization properties, better agreement is obtained. Note that the corrected sphere data are basically lower than those for the satellite and that the differences are greater for the shorter wavelengths (ultraviolet and blue). This suggests that some mechanism other than the ones which were investigated in the laboratory might be responsible for the differences such as solar ultraviolet radiation. This mechanism appears to be a likely candidate considering the findings of Clemmons and Camp (Ref. 13) that ultraviolet radiation causes the absorption properties of the Echo II material to decrease inversely with wave length.

The fact that the polarization data for the satellite produced curves with slopes more similar to those for the Echo II sphere than those for the aluminum substrate sphere indicates that the satellite's reflecting surface was basically the alodine coating on the

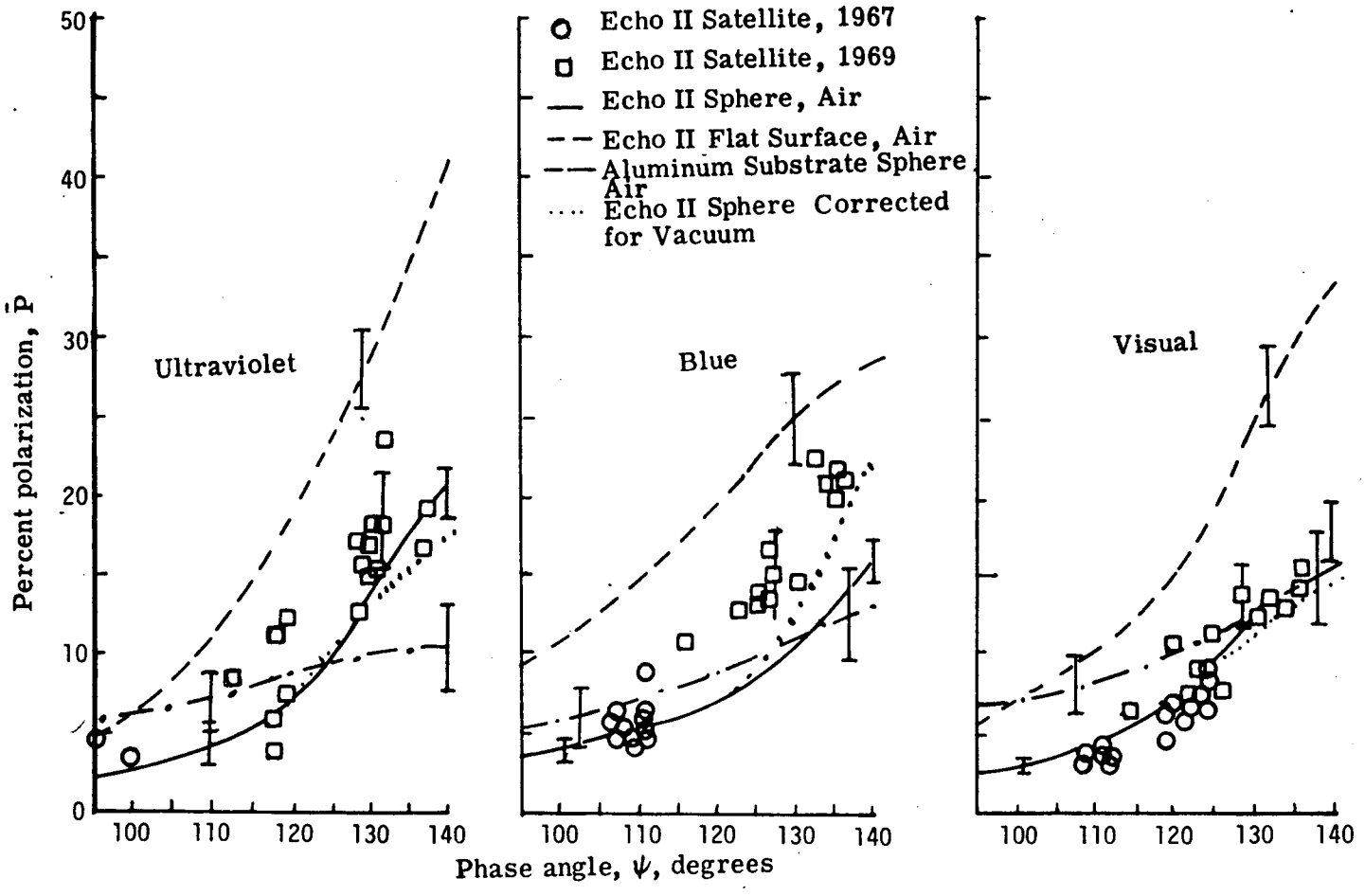

Figure 29.- Comparison of the Echo II Satellite measurements with the laboratory measurements.

aluminum substrate during the 1967 and 1969 observations.

PAGEOS I. - The polarization data for the PAGEOS I are given in figure (30) for the 1967 and 1969 observation periods. The satellite is found to have polarized the incident sunlight in increasing amounts in the ultraviolet, blue, and visual bands for phase angles greater than 100°. This is similar to the spectral polarization properties exhibited by the PAGEOS I material in the laboratory. The agreement between the satellite and laboratory data indicates that the surface of the PAGEOS I experienced little, if any, surface degradation in its first three years in space.

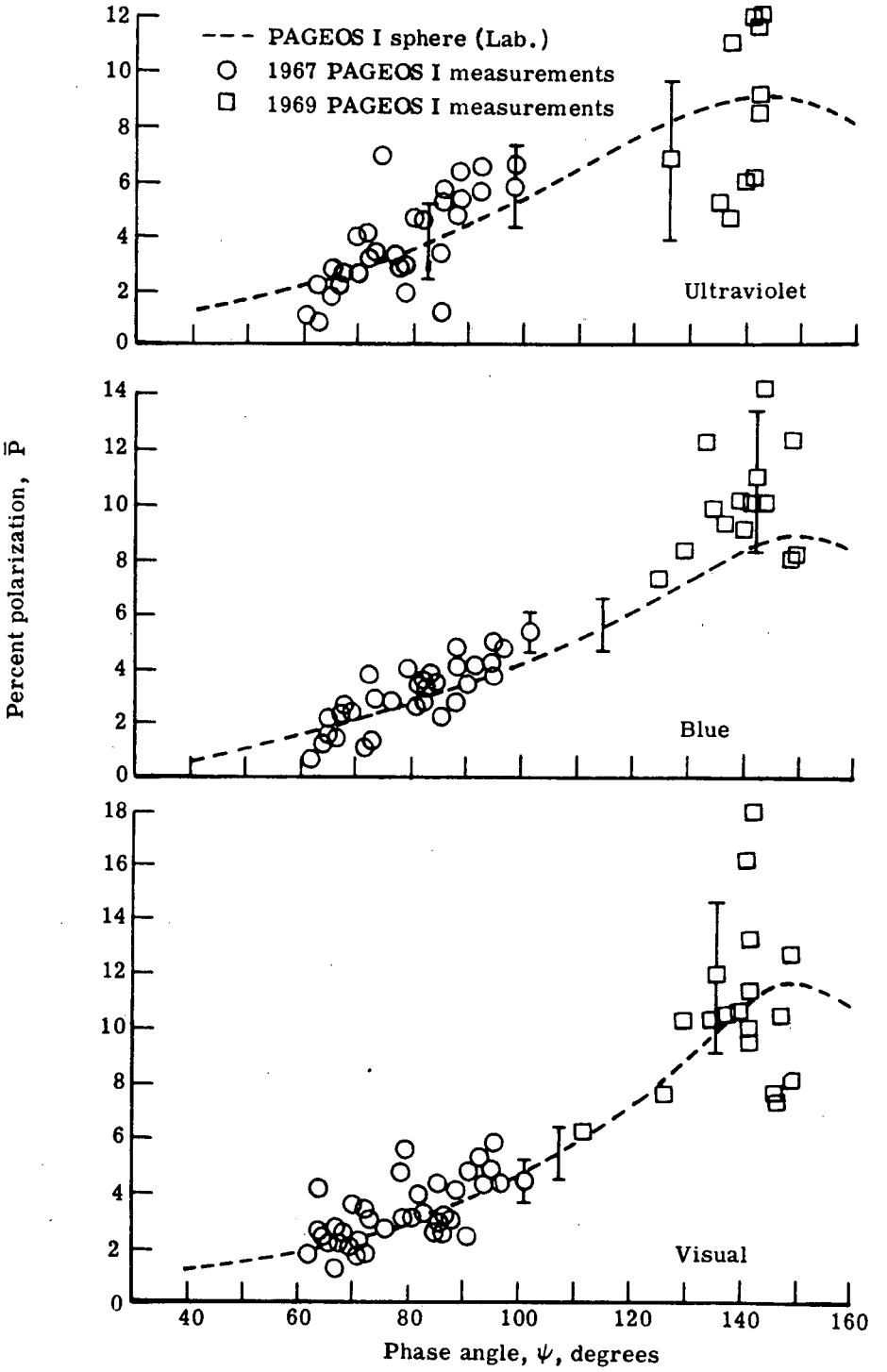

Figure 30.- Comparison of the polarimetric measurements of the PAGEOS I to those obtained in the laboratory (sphere).

CHAPTER VII

CONCLUDING REMARKS

The laboratory investigations of the light polarizing properties for flat test surfaces, representative of the Echo II and PAGEOS I, provided information essential to the analyses of the ground-based polarimetric measurements of the Echo II and PAGEOS I. In the laboratory, the effects of skin strain, surface geometry, and vacuum upon the optical properties of the test surfaces were examined. The results of the laboratory investigations support the following conclusions:

(1) The stress-relaxation tests revealed that pre-stressing the Echo II and PAGEOS I surface materials at 479 and 70 n/cm^2 respectively had no significant affect on the basic light polarizing properties of either surface.

(2) The polarization of light reflected from a test surface was found to be dependnet upon the geometric shape of the surface if the surface reflected a significant component of diffuse light compared to the component of specularly reflected light. Since the Echo II type surface reflects a large amount of diffuse light (Ref. 4), the sphere constructed of this material was found to polarize the light considerably less than the flat-shaped surfaces; however, it was found to polarize the light in increasing amounts in the blue, visual, and ultraviolet spectral bands, the same as the flat surfaces. In addition, the light diffusely reflected from the Echo II sphere was found to be polarized essentially in the plane of incidence, and to a greater degree than the

specularly reflected light. The sphere constructed of the PAGEOS I was found to polarize the incident light essentially the same as the flat surfaces since the material reflects about 87 percent of the incident light specularly and only three percent diffusely (Ref. 4).

(3) Vacuum (10^{-6} torr) was found to have a significant effect upon the polarization properties of the Echo II type material and no significant effect upon those of the aluminum surfaces. In vacuum, the Echo II surface was found to polarize the incident light more in the blue band and less in the ultraviolet and visual bands than it did in air. The surface, in vacuum, spectrally polarized the light in increasing amounts in the following order of spectral bands: visual, ultraviolet, and blue, which is different from the order (blue, visual, ultraviolet) exhibited by the surface in air (atmospheric pressure). The polarization changes were caused by the outgassing of water, changing the optical properties of the material's alodine coating.

Based upon the laboratory results, the analyses of the polarimetric measurements of the Echo II satellite and PAGEOS I suggest the following conclusions:

(1) The Echo II satellite experienced detectable changes in its optical surface during its five year lifetime in space. The surface changes were primarily caused by the outgassing of water vapor in space vacuum. It should be noted that the changes due to vacuum probably occurred within the first week of the satellite's lifetime in space. The fact that the polarization data for the satellite resembled the laboratory data indicates that the reflecting surface for the Echo II was essentially the alodine coated to aluminum.

(2) The PAGEOS I experienced no significant surface degradation in its first three years in space, indicating that aluminum is optically stable in space.

REFERENCES

1. Jakes, William C., Jr.: Participation of Bell Telephone Laboratories in Project Echo and Experimental Results. NASA TN D-1127, December 1961.

2. Bowker, David E.: PAGEOS Project - Compilation of Information for Use of Experimeter. NASA TM X-1344, March 1967.

3. Mobile 24-Inch Satellite Photometric Observatory. NASA CR-66304, October 1966.

4. Romick, D. C., et al., The Modification and Use of a Ground-Based Photometer for Evaluation of Satellite Materials, NASA CR-66772, 1968.

5. Romick, D. C., R. H. Emmons, and R. J. Preski, Evaluation of Satellite Materials by Use of Ground-Based Photometric Observatory-Phase II, NASA CR-66899, 1969.

6. Ditchburn, R. W.: Light, Second ed., Interscience Publ., Inc., c. 1963.

7. Beckman, Peter; and Spizzichino, André: The Scattering of Electromagnetic Waves from Rough Surfaces. The Macmillian Company, c. 1963.

8. McCoyd, G. C.: Polarization Properties of a Simple Dielectric Rough Surface Model. Journal of the Optical Society of America, vol. 57, no. 11, November 1967, pp. 1345-1350.

9. Tousey, R.: The Visibility of An Earth Satellite. Astronautic Acta, vol. II, no. 2, 1956, pp. 101-112.

10. Tousey, R.: Optical Problems of the Satellite Journal of the Optical Society of America, vol. XLVII, 1957, p. 261.

11. Russell, H. N.: On the Albedo of the Planets and Their Satellites. Astrophysical Journal, vol. XLIII, April 1916, p. 173.

12. Dollpus, Audoium: Polarization Studies of Planets. (Planets and Satellites (Edited by G. P. Kuiper and B. M. Middlehurst), University of Chicago Press, 1961, p. 368.

13. Clemmons, Dewey L., Jr.; and Camp, John D.: Amorphous Phosphate Coatings for Thermal Control of Echo II. Electrochemical Technology, vol. 2, no. 7-8, July-August 1964, pp. 221-231.

14. Teichman, Louis A.: The Fabrication and Testing of PAGEOS I. NASA TN D-4596, June 1968.

15. Price, Howard L.; and Pezdirtz, George F.: Mechanical Properties of Echo II Laminate. NASA TN D-2367, August 1964.

16. Lee, Robert B., III: Optical Polarimetric Properties of the Materials in the PAGEOS I and Echo II Satellite Surfaces. NASA TM X-2089, September 1970.

17. Anon: Handbook of Chemistry and Physics. Thirty-seventh edition, Chemical Rubber Publishing Company, 1955, p. 2,678.

18. Kampensky, A.; and Ritt, R. K.: Experimental and Theoretical Evaluation of a Passive Communications Satellite (Echo II). NASA TN D-3154.

19. Bahiman, Hossenin: Post Structural Analysis of Echo II Satellite. NASA TN D-3170, February 1966, p. 1.

20. Bassalera, N. Ia: Evolution of Gas in Metals Used in Vacuum Technology. Soviet Physics, vol. 3, no. 5, May 1958, pp. 1027-1031.

21. Behr, Alfred: "Die Interstellar Polarization Des Sternliches In Sonnenumgebung," Nochrichten Der Akerdemic-Wissenchaffen In Gottingen In Mathematish-Physikalishe Klasse, Venderhoeck and Ruprecht, Gottingen, 1959.

APPENDIX A

DETERMINATION OF PLANE OF POLARIZATION

Generally, the plane of polarization, containing the polarized component of the light, is defined with respect to the plane of incidence (defined by the directions of the incident and reflected light beams) by the angle of polarization η. During a satellite observation, the plane of polarization was defined with respect to a reference plane (containing the declination axis of the telescope) by the angle η_1 (see figure 18). In order to define, the orientation of the plane of polarization to the plane of incidence, the orientation of the reference plane with respect to the plane of incidence had to be defined, and this is done with the aid of spherical trigonometry.

Consider the positions of the satellite and sun as illustrated in figure A-1. Sat represents the position of the satellite on the celestial sphere at the time of interest while sun denotes the position of the antipodal sun, diametrically opposite the true position of sun. Using the altitude-azimuth system, the observer is located at the center of the sphere with his local zenith Z directly overhead, and his horizon located 90° away from the zenith and represented by the horizontal plane. N' represents the north pole of the reference plane which passes through the position of the satellite, sat. The phase angle of the satellite at the time of interest is denoted by ψ, and lies in the plane of incidence. The angle "b" defines the orientation of the reference plane to the plane of incidence while ψ_{min} denotes the

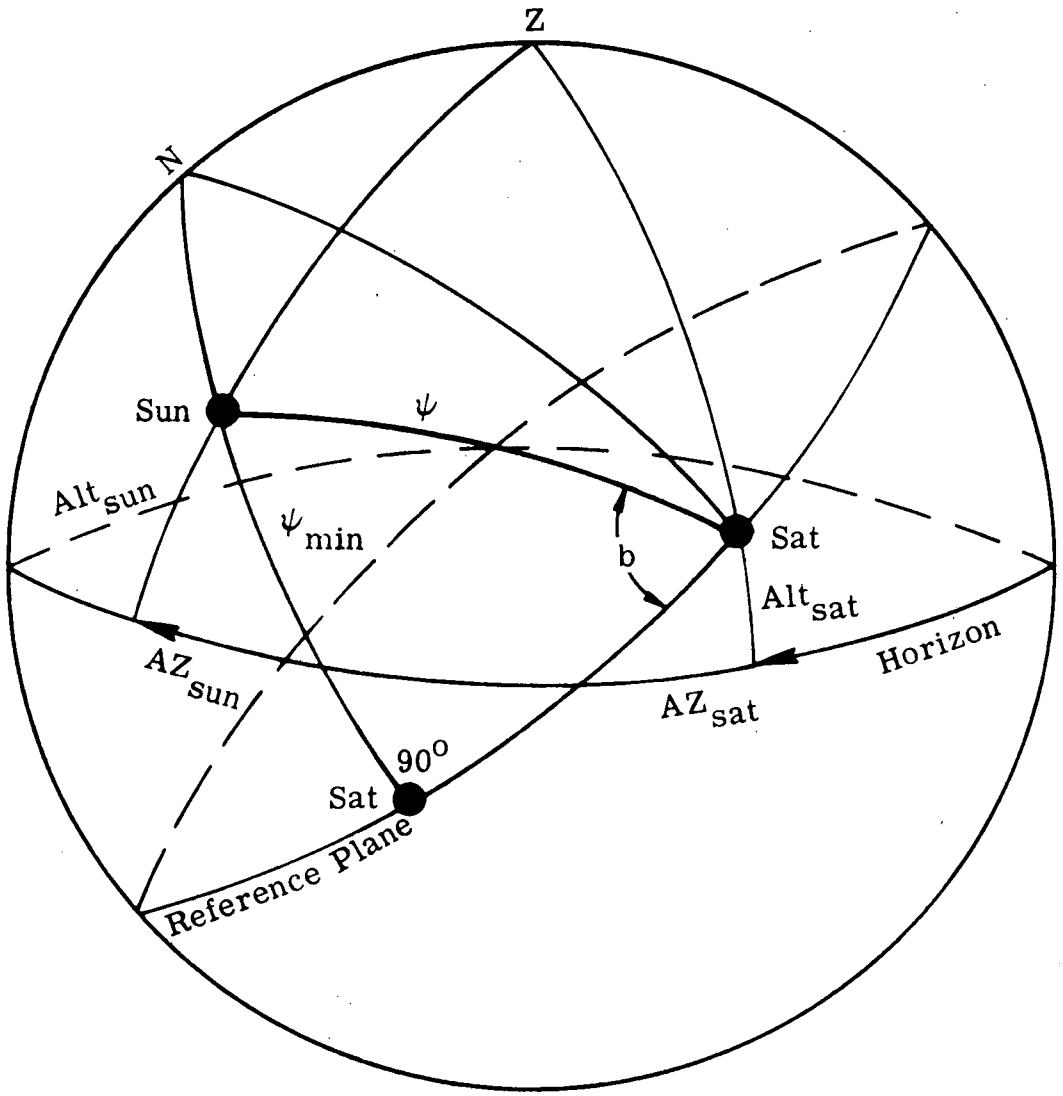

Figure A.1 - Orientation of the plane of polarization.

minimum phase angle where the plane of incidence is perpendicular to the reference plane. Looking at the triangle containing "b", ψ, and ψ_{min}, "b" is calculated using the law of sines for a spherical triangle

$$\sin(b) = \frac{\sin 90^{o} \text{ X } \sin (\psi_{min})}{\sin \psi} \qquad \text{A-1}$$

Finally, the calculated value of "b" is subtracted from η_1 in order to determine the true angle of polarization η

$$\eta_1 - b \qquad \text{A-2}$$

which defines the orientation of the plane of polarization with respect to the plane of incidence.